ANL-76-133

TRITIUM PROCESSING AND CONTAINMENT TECHNOLOGY FOR FUSION REACTORS ANNUAL REPORT

July 1975—June 1976

by

V. A. Maroni, W. F. Calaway, B. Misra,
E. H. Van Deventer, J. R. Weston,
R. M. Yonco, F. A. Cafasso, and L. Burris

U of C-AUA-USERDA

ARGONNE NATIONAL LABORATORY, ARGONNE, ILLINOIS

Prepared for the U. S. ENERGY RESEARCH AND DEVELOPMENT ADMINISTRATION under Contract W-31-109-Eng-38

Printed in the United States of America
Available from
National Technical Information Service
U. S. Department of Commerce
5285 Port Royal Road
Springfield, Virginia 22161
Price: Printed Copy $4.50; Microfiche $3.00

Distribution Category:
Controlled Thermonuclear Processes
and Plasma Physics
(UC-20)

ANL-76-133

ARGONNE NATIONAL LABORATORY
9700 South Cass Avenue
Argonne, Illinois 60439

TRITIUM PROCESSING AND CONTAINMENT TECHNOLOGY FOR FUSION REACTORS ANNUAL REPORT

July 1975—June 1976

by

V. A. Maroni, W. F. Calaway, B. Misra, E. H. Van Deventer,
J. R. Weston, R. M. Yonco, F. A. Cafasso,
and L. Burris

Chemical Engineering Division

Previous reports in this series

ANL-8023	January—June 1973
ANL-8123	July 1973—June 1974
ANL-75-50	July 1974—June 1975

TABLE OF CONTENTS

LIST OF FIGURES

LIST OF TABLES

TRITIUM PROCESSING AND CONTAINMENT TECHNOLOGY FOR FUSION REACTORS ANNUAL REPORT

July 1975—June 1976

by

V. A. Maroni, W. F. Calaway, B. Misra, E. H. Van Deventer, J. R. Weston, R. M. Yonco, F. A. Cafasso, and L. Burris

ABSTRACT

The hydrogen permeabilities of selected metals, alloys, and multiplex preparations that are of interest to fusion reactor technology are being characterized. A high-vacuum hydrogen-permeation apparatus has been constructed for this purpose. A program of studies has been initiated to develop design details for the tritium-handling systems of near-term fusion reactors. This program has resulted in a better definition of reactor-fuel-cycle and enrichment requirements and has helped to identify major research and development problems in the tritium-handling area. The design and construction of a 50-gallon lithium-processing test loop (LPTL) is well under way. Studies in support of this project are providing important guidance in the selection of hardware for the LPTL and in the design of a molten-salt processing test section.

SUMMARY

Experimental Studies of Tritium Barrier Concepts

Developmental work is continuing on tritium containment and control methodology that would be applicable to a variety of fusion power reactor environments. A high-vacuum system which utilizes a mass spectrometer to measure hydrogen flow rates is described. This system was used to obtain permeation data on vanadium, Haynes-188, and two stainless steel multiplexes containing aluminum bronze.

Assessment of the Tritium Containment and Processing Requirements for Experimental Fusion Devices

A design has been developed for the fuel recycle and processing systems of an experimental fusion power reactor (EPR). This study included analyses of the fuel recycle composition and flow rate, the disposition and total inventory of tritium, and the requirements for atmospheric detritiation systems. A computer program was written to calculate operating characteristics of the cryogenic distillation cascade used to separate protium and adjust deuterium/tritium ratios. Similar design studies were also carried out for a Tokamak engineering technology facility (TETF).

Development of Liquid Lithium Processing Technology

A program of studies aimed at developing methods of recovering tritium from fusion reactor blanket materials has focused on a molten-salt extraction process for removing tritium from liquid lithium. Experiments were conducted to evaluate both gas sparging and electrochemical techniques as possible methods of recovering hydrogen isotopes from the extractant salt. In light of encouraging bench-scale results and in an effort to examine lithium processing on a larger scale, design of a 50-gallon liquid lithium processing test loop (LPTL) has been initiated. In addition, a 1-liter lithium mini-test loop has been fabricated in support of the LPTL. Results of efforts in each of these areas are summarized below.

Gas-Sparging Studies: Sparging experiments have been performed to recover hydrogen and deuterium (in lieu of tritium) from molten mixtures of LiCl-KCl and LiF-LiCl-LiBr, using HCl as the reactive gas. From studies in which LiCl-KCl was used as the salt medium, it is concluded that this particular salt mixture is not acceptable for large-scale molten-salt processing because of the reduction of the potassium cation by lithium. Sparging experiments with LiF-LiCl-LiBr were very successful. Complete removal of both hydrogen and deuterium from the salt was observed at the <5 wppm level. The complication of having the salt saturated with metallic lithium does not interfere with the extraction process beyond requiring additional amounts of HCl to remove the metal by reaction. With futher optimization and refinement of the processing methodology, it is reasonable to expect that the steady-state levels of hydrogen isotopes in a lithium loop can be maintained at <1 wppm by a molten-salt extraction process which uses sparging to reprocess the salt.

Electrochemical Studies: Experiments are presently under way to develop the methodology for electrochemical extraction of hydrogen isotopes from hydride solutions in molten salts. To date, extraction of deuterium from LiF-LiCl-LiBr has been accomplished down to 1 wppm, using a graphite electrode in one series of experiments and a graphite electrode coated with a ceramic in another series. From the results of these experiments, it is apparent that electrolysis is a viable means for reprocessing the molten salt and most likely will be preferred over sparging as the method for recovering hydrogen isotopes from molten-salt extractants.

Lithium-Processing Test Loop: A multipurpose lithium-processing test loop (LPTL) has been designed. This 50-gallon forced-circulation loop will (1) test the effectiveness of semi-continuous molten-salt extraction, using a single vessel as a pseudo mixer-settler; (2) evaluate the efficiency of an elevated-temperature getter trap and a thermally regenerative cold trap for removing nonmetallic element impurities from lithium; and (3) develop impurity control, process, and monitoring methodology for large liquid lithium loop systems. The facility is being fabricated from 304L stainless steel and will operate at or below 550°C. Construction of the loop components is under way and operation is expected to begin in the fall of 1977.

Lithium Mini-Test Loop: A liquid-metal mini-test loop having a capacity of about one liter of lithium has been constructed and put into operation. The loop will be used to develop information in support of the design of the lithium-processing test loop (LPTL) in the areas of valve performance, hot

gettering of nitrogen, and liquid-metal sampling procedures. The loop is made of Type 304 and 316 stainless steel components, and has an overall space requirement of 2 by 3 by 4 ft. Operation of the loop should begin in September 1976.

I. INTRODUCTION

The work described in this report is directly supportive of the controlled thermonuclear research program currently sponsored by the ERDA Division of Magnetic Fusion Energy. Previous progress reports covering the work are identified in Refs. 1-4. Reported below are results of (1) efforts to develop and characterize permeation-resistant metal multiplexes for high-temperature applications in fusion reactor systems, (2) analyses of the tritium-handling requirements for a Tokamak experimental power reactor, (3) bench-scale studies of tritium-recovery concepts for liquid lithium blankets, and (4) efforts to design a 50-gal lithium-processing test facility.

II. EXPERIMENTAL STUDIES OF TRITIUM BARRIER CONCEPTS
(E. H. Van Deventer, B. Misra, and V. A. Maroni)

Developmental work is continuing on tritium containment and control methodology that would be applicable to a variety of fusion power reactor environments. The motivation for this research program has been discussed previously.[1,5,6] A major programmatic objective is to prepare and characterize individual materials and composites of materials with low hydrogen permeabilities as compared with the permeabilities of conventional structural alloys (*e.g.*, stainless steels).

A. Experimental Apparatus and Methods

A diagram of the equipment currently employed for permeation measurements is shown in Fig. 1. This apparatus consists of two all-metal high-vacuum compartments interconnected by a membrane assembly containing the material to be studied. Each compartment contains a liquid-nitrogen-cooled cryosorption pump, an ion pump, and a bakeable ion gauge. The upstream compartment also contains a hydrogen-isotope supply system consisting of a heated silver-palladium thimble and an automatic pressure controller that is electrically interfaced with the pressure measuring device (a capacitance manometer). The downstream compartment is equipped with a cycloidal mass spectrometer, a nonevaporable getter pump, and three standard hydrogen leaks. The material under study is heated by a clamshell furnace. After an equilibrium hydrogen flow has been established through the membrane, measurements are made by alternately valving off the appropriate standard leak(s) and the membrane assembly. The output of the mass spectrometer, tuned to the hydrogen (mass 2) peak, is continuously monitored with an X-Y recorder. Permeation rates are obtained by ratioing the resultant steps or changes in the partial pressure of hydrogen that occur when the sample and/or standard leak(s) are valved off. By operating in this dynamic (continuous pumping) mode, the apparatus is currently capable of measuring hydrogen flow rates in the range from 1×10^{-4} to 5×10^{-9} cm^3 (STP)/s.

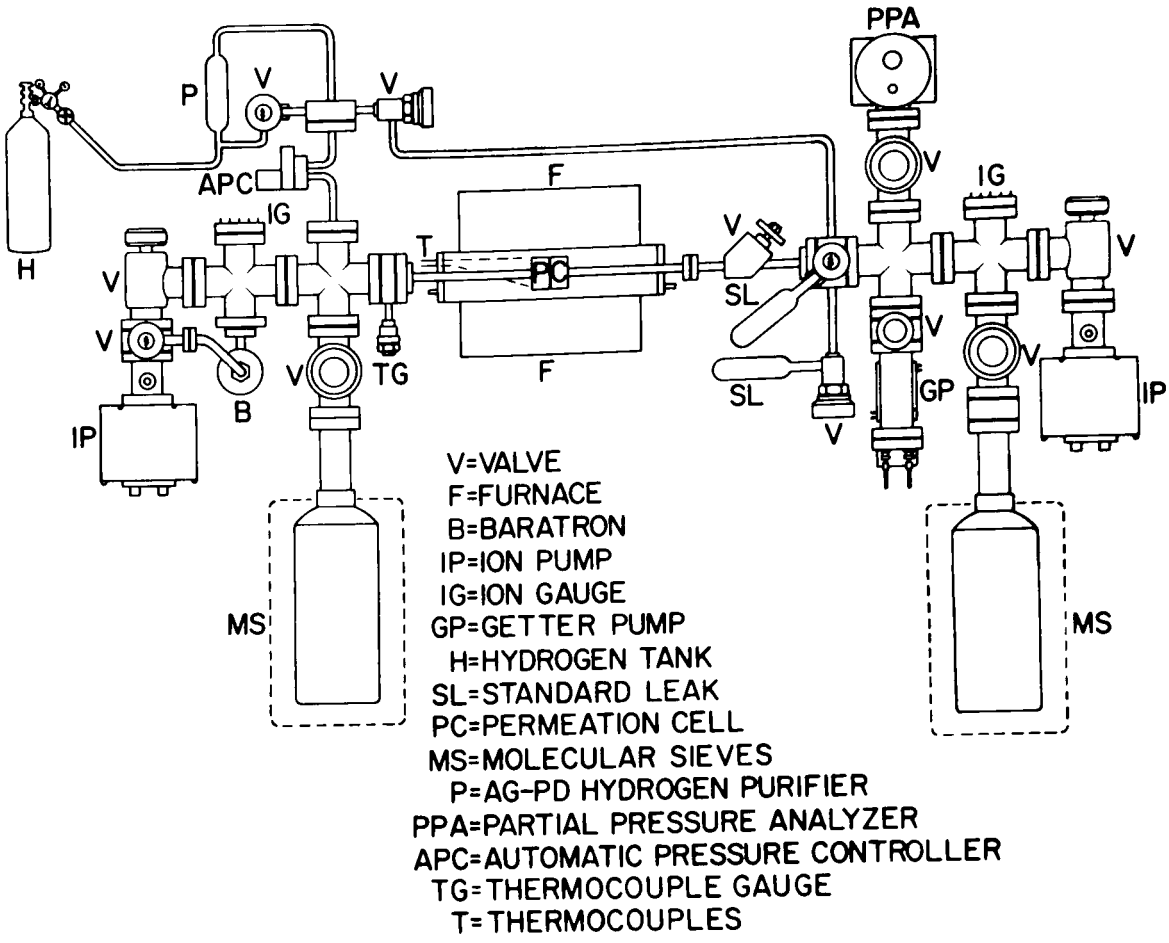

Fig. 1. Hydrogen Permeation Apparatus

B. Studies of Hydrogen Permeation Through Vanadium

Initial permeation measurements with the equipment described above were made with vanadium in order to resolve uncertainties that existed in previous measurements of permeation through vanadium.[5,7,8] Recent data, identified chronologically in Fig. 2, exhibit considerable scatter. Also included in Fig. 2 are the extrapolated data of Heinrich *et al.*[8] and our earlier results for heavily oxidized vanadium.[7] Comparison of the results in Fig. 2 suggests that, under improved vacuum conditions, the long-term effects of impurities become significant only below 325°C. (Above 325°C, the measured permeability in the cleaner vacuum approaches the extrapolated data of Heinrich *et al.*[8]) We have therefore concluded that vanadium used as a fusion reactor construction material would have a manageably low hydrogen permeability only if a surface impurity layer could be maintained on at least one surface without simultaneously destroying the bulk material.

In another area of investigation, some earlier uncertainties were resolved regarding oxygen distribution profiles in vanadium samples subjected to long-term hydrogen permeation. Results of an earlier investigation[5] using ion microprobe mass analyzer methods had indicated that the oxygen levels near the surface of some vanadium permeation samples that had been studied for months were well below 1 wt %, even though microscopic

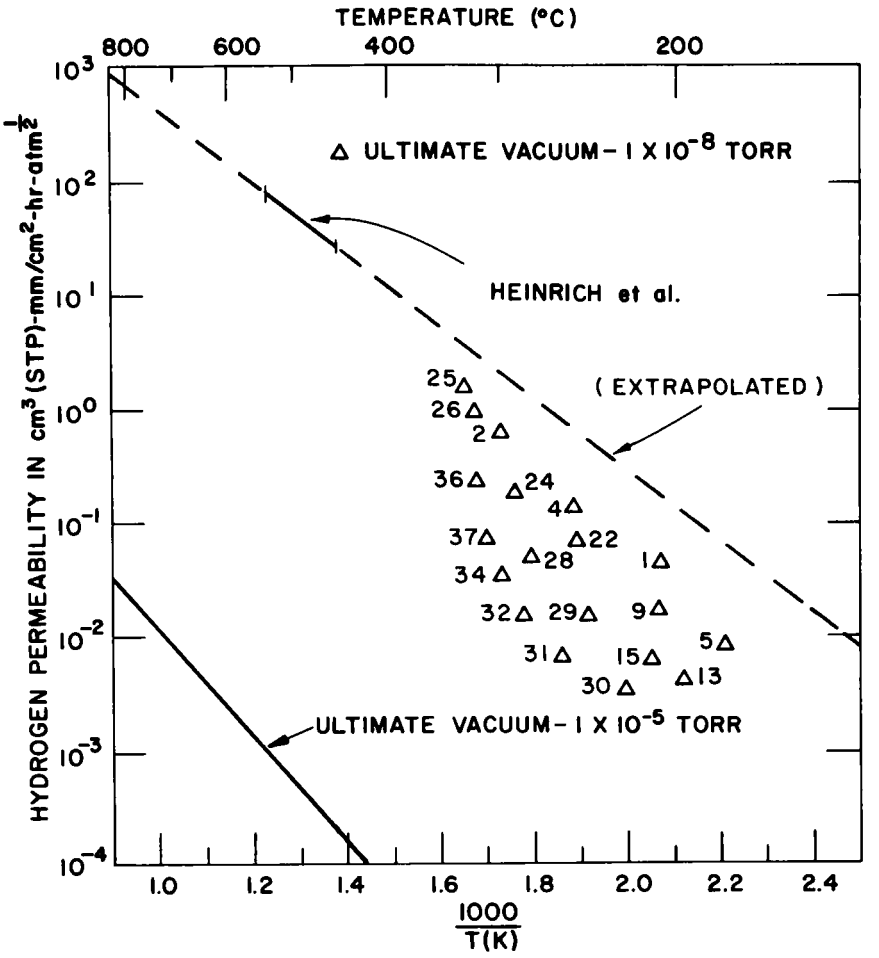

Fig. 2. Hydrogen Permeability of Vanadium for Various Background Impurity Cases. (Numbers indicate approximate day of run for the study with the high-vacuum apparatus.)

examination gave evidence of the presence of nearly pure oxide layers. A reexamination of several of the same samples carried out by Grumman Aerospace Corporation using nuclear microprobe methods[9,10] revealed that the discrepancy lay in the assumptions used to calibrate the ion microprobe data; *i.e.*, the oxygen level near the surface of the as-received reference material as determined by the nuclear microprobe was found to be nearly an order of magnitude higher than the lot analysis value determined on bulk samples of the same material. Revised oxygen depth profile data are given in Fig. 3. The agreement among data from ion microprobe, nuclear microprobe, and microscopic analyses is now found to be in good accord. The reader is referred to Ref. 11 for a more comprehensive discussion of the results in Fig. 3.

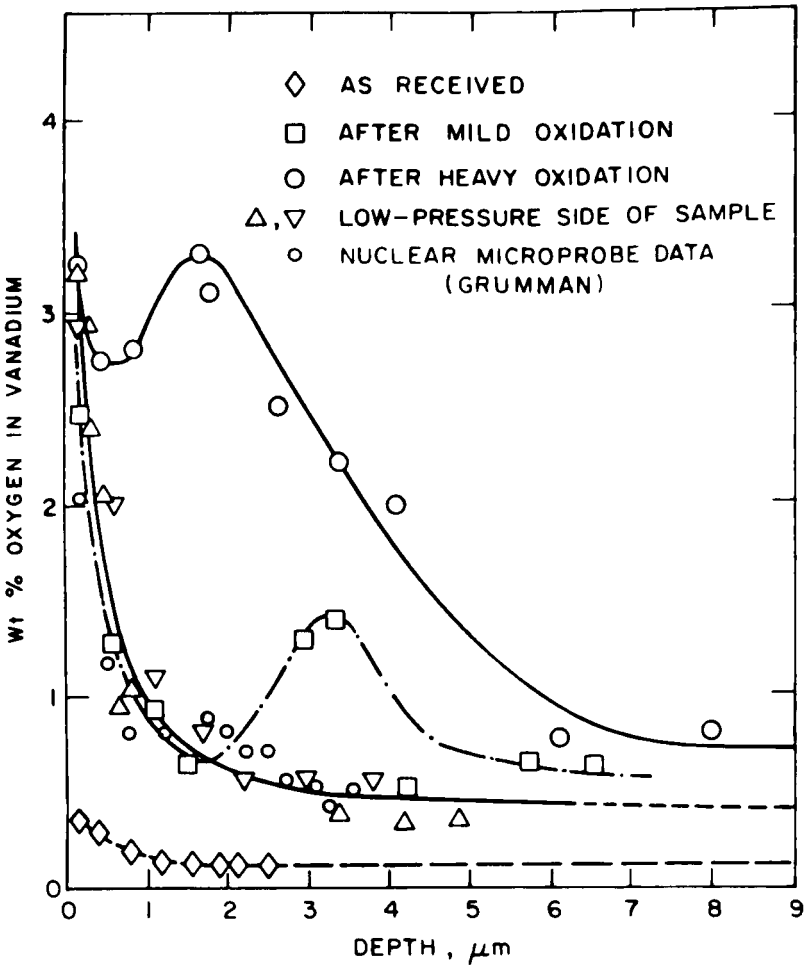

Fig. 3. Ion Microprobe Data on Weight Percent Oxygen *vs.* Depth.

C. Cladding Concepts for Advanced Refractory Alloys

Since vanadium-base alloys are leading candidates as liquid-lithium containment materials for lithium-blanketed fusion power reactors and in light of the results reported in Ref. 11, there is sufficient incentive to search for cladding alloys (for the exterior surfaces of vanadium structures) that are air-stable at elevated temperatures (600 to 1000°C). The Haynes series of alloys offers a potentially useful class of materials for this application because their upper operating temperature limit in air is in excess of 1000°C. If we assume that the hydrogen permeability of vanadium in a Haynes alloy/vanadium/liquid lithium configuration remains relatively high[11] over extended operating times, the question of further tritium permeation through the cladding alloy becomes significant. Figure 4 shows the results of a hydrogen permeation study carried out in our laboratory for Haynes 188 (38 wt % Co, 22 wt % Ni, 22 wt % Cr, 14.5 wt % W, 3 wt % Fe, 0.15 wt % C, 0.15 wt % La). The results were obtained for upstream hydrogen pressures in the range from 0.3 to 180 torr and temperatures in the range from 210 to 710°C. Over this entire range of temperatures and

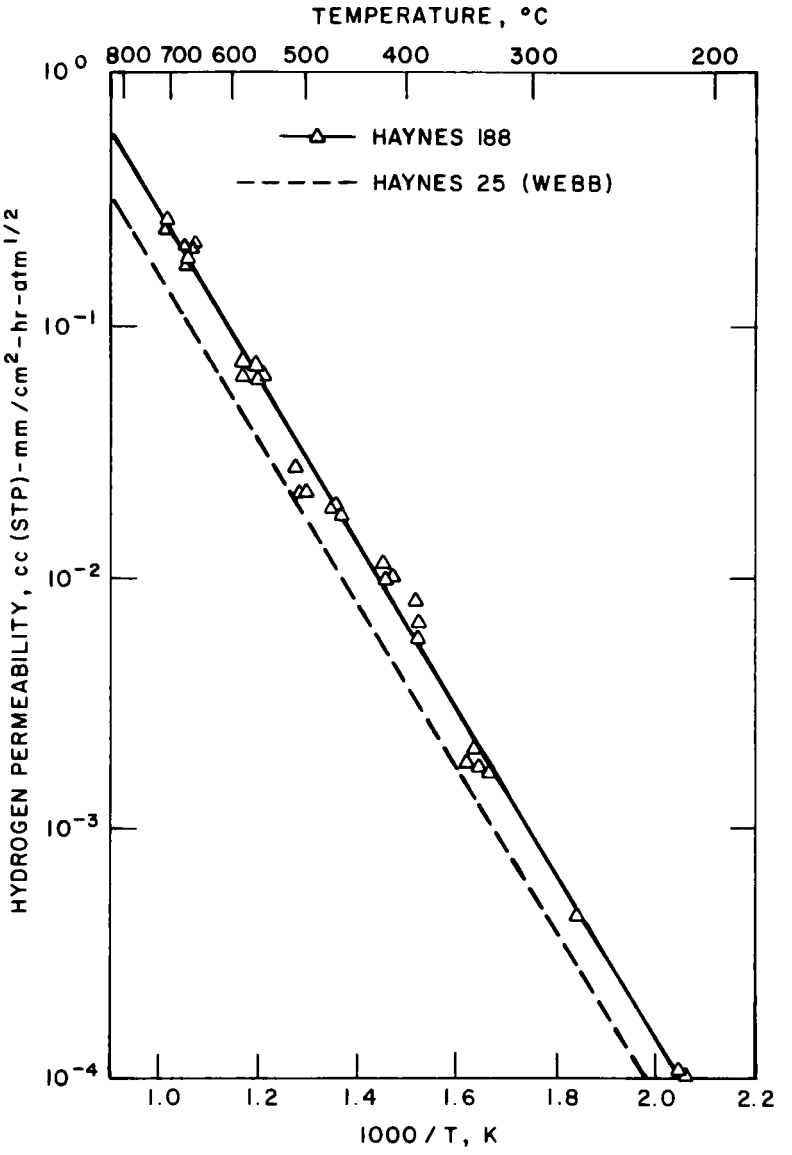

Fig. 4. Hydrogen Permeation Data for Haynes-188 (this study) together with Least-Squares Refined Permeability Curves for Haynes-188 and Haynes-25 (Webb, Ref.12).

pressures, the rate of permeation was found to be proportional to the half-power of the hydrogen driving pressure (0.5 ± 0.05), as shown in Fig. 5. The permeation curve for Haynes 25 as reported by Webb[12] is also included in Fig. 4 for comparison purposes. The hydrogen permeabilities of these alloys are in the same range as that for most conventional austenitic alloys (see, for example, Refs. 5 and 12) and can be represented by the following equations:

$$\Phi(\text{Haynes 188}) = 545 \exp(-15{,}040/RT),\ \text{cm}^3(\text{STP})\cdot\text{mm}/\text{cm}^2\cdot\text{hr}\cdot\text{atm}^{1/2}$$

$$\Phi(\text{Haynes 25}) = 327 \exp(-15{,}100/RT),\ \text{cm}^3(\text{STP})\cdot\text{mm}/\text{cm}^2\cdot\text{hr}\cdot\text{atm}^{1/2}$$

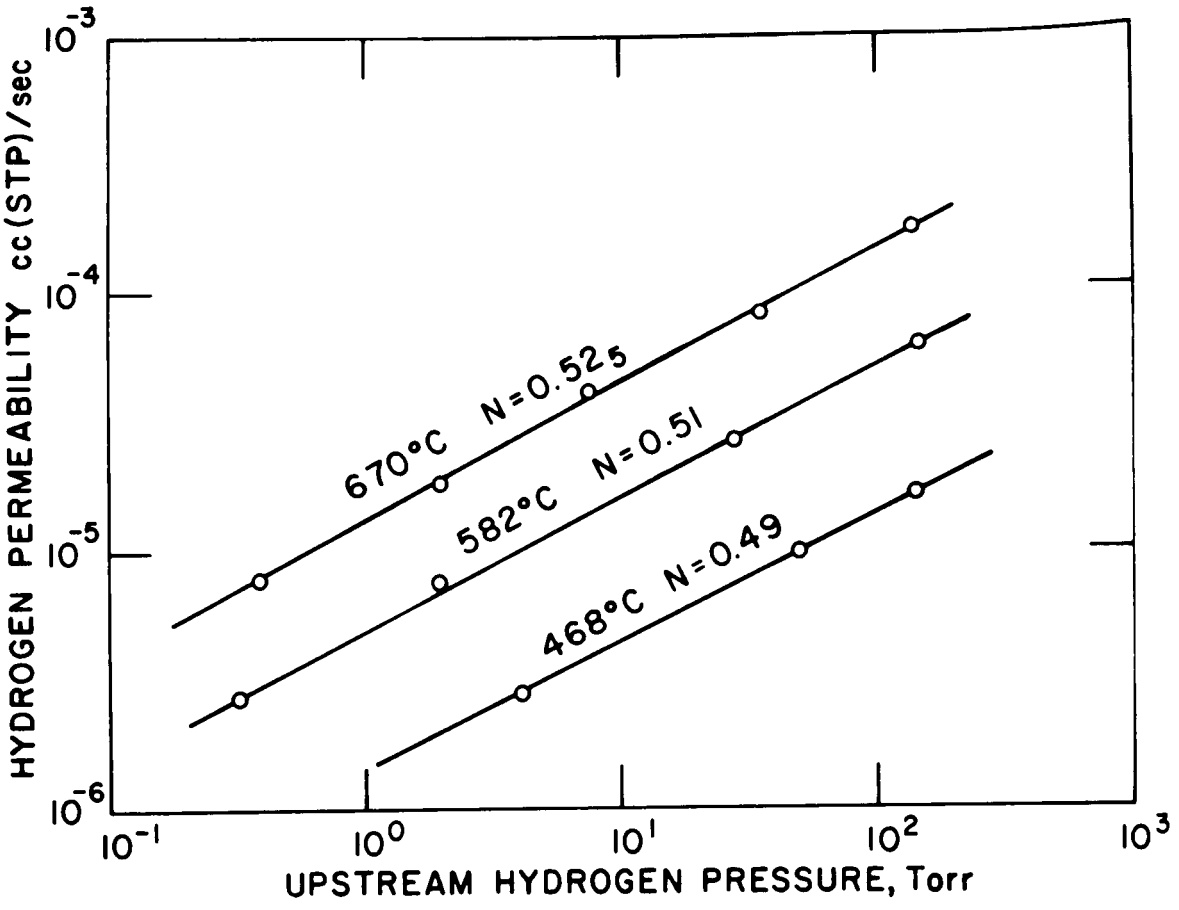

Fig. 5. Log-Log Plot of Hydrogen Permeation Rate *vs.* Upstream Hydrogen Pressure for Haynes-188 at 670, 582, and 468°C; N = Slope. (The correlation coefficient for each set of data was better than 0.995 in the least-squares analysis.)

Depending on the actual permeability of vanadium in the cladding configuration discussed above, the rate of hydrogen permeation through a Haynes 188 or 25 cladding could approach that which would be obtained if the vanadium were not even present. At temperatures above 500°C, the need for additional permeation barriers in Haynes-clad vanadium structures appears to be essential. However, it is important to note that the effects of air oxidation on the exterior surfaces of the Haynes alloys might lead to increased permeation resistance if, for example, stable oxide layers can be made to persist.

D. Development of Bronze Permeation Barriers

An effort is currently under way at ANL to explore methods for reducing tritium permeation in near-term confinement experiments and in future fusion power reactors. The methods being studied include (1) multiplex metal structures containing at least one layer of a material that is relatively impermeable to hydrogen isotopes and (2) ceramic and other special coatings on structural metal surfaces. The objectives, general approach, and

experimental procedures used in this program were described in previous publications.[5,6] A major finding of the studies carried out to date has been that aluminum bronze (10 wt % Al; 4 wt % Fe; balance, Cu), a commercially available high-strength corrosion-resistant copper alloy, develops appreciable resistance to hydrogen permeation on standing in relatively clean environments at elevated temperatures.[5] Because of the substantial technology base that exists with respect to the preparation of mechanically and metallurgically bonded copper/stainless steel composites, current efforts are focusing on the use of aluminum bronze as a permeation inhibitor in stainless steel systems.

Recent experiments have been directed towards examination of the permeation characteristics of metallurgically bonded aluminum bronze/304-SS multiplexes. Two such metallurgical multiplexes, a 304-SS/aluminum bronze sample and a 304-SS/aluminum bronze/304-SS sample, prepared by the ANL Materials Science Division, were subjected to hydrogen permeation using the all-metal high-vacuum system described in Ref. 11. The hydrogen permeability of both samples was found to drop from a value near that expected for a comparably thick piece of pure stainless steel to a value some 30 times lower over a period of a few weeks. Examination of the 304-SS/aluminum bronze/304-SS multiplex after permeation experiments showed that the sample had delaminated at both interfaces and that, in spite of the completely weld-enclosed nature of the interface regions (see Ref. 5 or 11 for sample configuration), both surfaces of the bronze inner layer were visibly oxidized. A similar delamination of the 304-SS/aluminum bronze duplex also occurred.

Results for the 304-SS/aluminum bronze duplex are shown in Fig. 6. In the study of this duplex, the sample was initially oriented with the bronze layer facing the downstream side of the permeation apparatus (an extremely clean environment in our system), but after nearly two months of study, the sample was reversed so that the bronze layer faced the upstream side. Little change in permeation rate was observed for the reversed sample when the results were compared with the lowest curve in Fig. 6.

The observed reduction in hydrogen permeation rate for the aluminum bronze multiplexes over the course of the permeation measurements was assumed to be associated with the delamination and subsequent surface oxidation of the bronze. The cause of the delamination was attributed to (1) inadequate surface cleaning prior to the bonding step and/or (2) reduction in metallurgical interface integrity due to the presence of aluminum. The studies do show that the low permeability of aluminum bronze is not a bulk property of the alloy but rather is due to the formation of surface impurity layers -- probably aluminum oxide or a ternary oxide. In current barrier-development studies, emphasis is on the identification and characterization of methods for applying adherent coatings of aluminum bronze or related aluminum-base materials to stainless steel.

E. Study of Interfacial Thermal Resistances for Metal Composites

In D-T-burning fusion reactors, permeation of tritium through structural materials presents numerous, difficult problems associated with tritium release to the environment, contamination of coolant and purge gas streams, contamination of work environment with radioactive tritium, etc. Of the

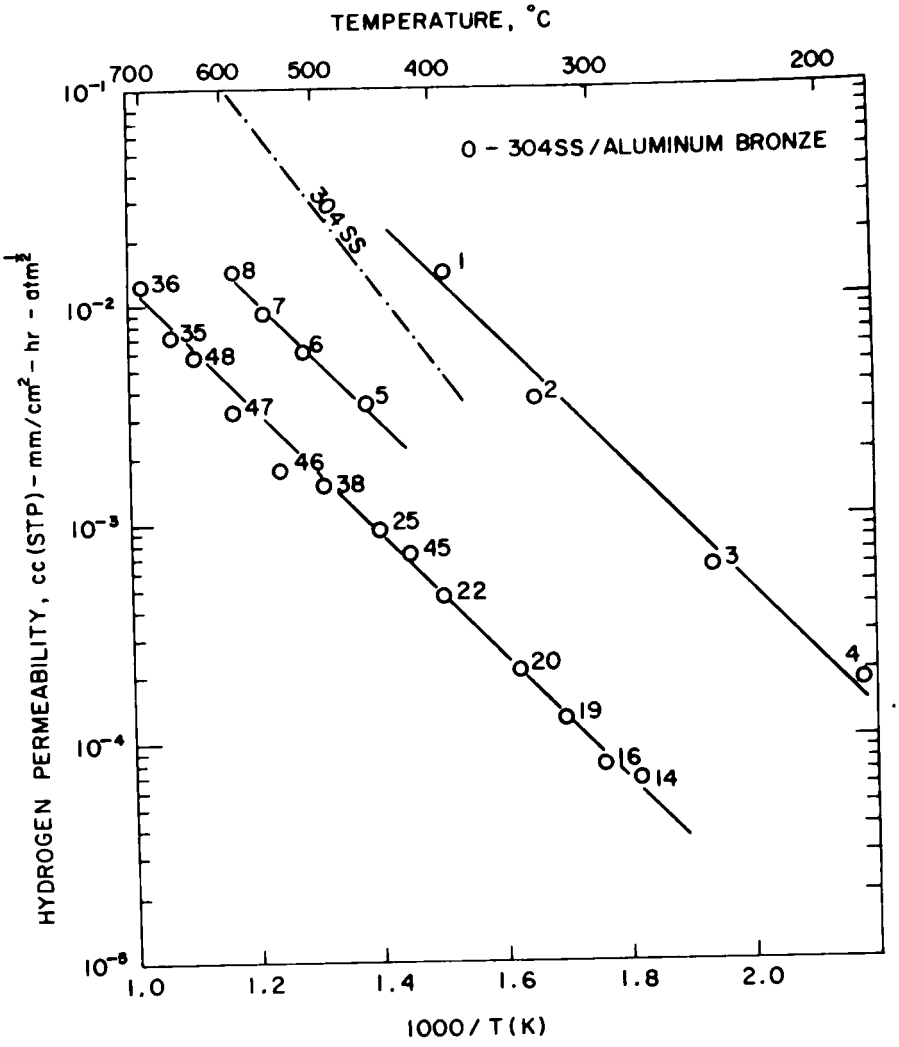

Fig. 6. Hydrogen Permeation Data for a Metallurgically Bonded 304-SS/Aluminum Bronze Multiplex. (Numbers indicate chronological order of measurements.)

several plausible methods for minimizing tritium permeation, metal composites appear to have attractive features. One aspect of the utility of composites that needs careful evaluation is the possible adverse effect on heat-transfer characteristics. When the physical contact between two heat-conducting surfaces is less than perfect, the interfacial thermal resistance can become a dominant factor in controlling thermal energy transport.

In this study, no attempt has been made either to analyze or investigate the fundamental nature of interfacial thermal resistance; rather, interfacial thermal resistances were measured for a mechanically bonded stainless steel/copper/stainless steel composite tubing over a range of temperatures. The steady-state heat conduction through a hollow cylinder (see Fig. 7) may be expressed as

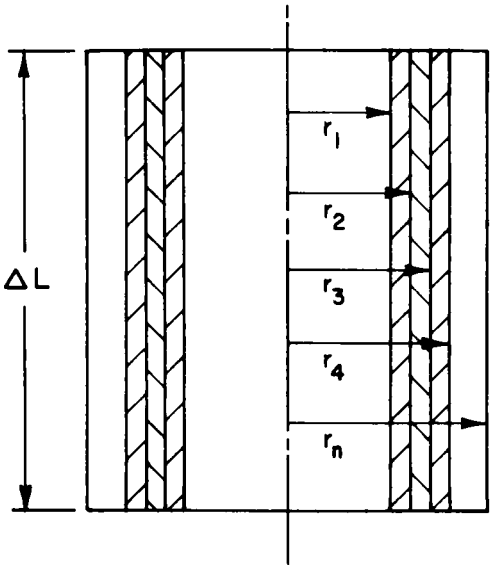

Fig. 7. Schematic of a Composite Sample

$$Q = \frac{T_2 - T_2}{\ln\left(\frac{r_2}{r_1}\right)/(2\pi K_{m1}\Delta L)} \cdots = \frac{T_{n-1} - T_n}{\ln\left(\frac{r_n}{r_{n-1}}\right)/(2\pi K_{mn}\Delta L)} \cdots \quad (1)$$

where

Q = heat flow rate, Btu/hr

K_{m1} = average thermal conductivity of sample, corresponding to temperatures T_1 and T_2, Btu/hr·ft·°F

K_{mn} = average thermal conductivity of sample, corresponding to temperatures T_{n-1} and T_n, Btu/hr·ft·°F

$r_1, r_2 \ldots r_n$ = radii of the layers of sample, ft

$T_1, T_2 \ldots T_n$ = temperatures of sample corresponding to $r_1, r_2 \ldots r_n$, respectively, °F

ΔL = length of sample, ft

For a three-layer SS/Cu/SS composite, Eq. 1 becomes (after eliminating the intermediate temperatures):

$$Q = \frac{T_1 - T_4}{\frac{\ln\left(\frac{r_2}{r_1}\right)}{2\pi K_1 \Delta L} + \frac{\ln\left(\frac{r_3}{r_2}\right)}{2\pi K_2 \Delta L} + \frac{\ln\left(\frac{r_4}{r_3}\right)}{2\pi K_3 \Delta L}} \cdots \quad (2)$$

$$= \frac{\Delta T}{R_1 + R_2 + R_3} \cdots \quad (3)$$

where $\Delta T = T_1 - T_4$, and R_1, R_2 and R_3 are the thermal resistances of the three layers of the composite. To compare the thermal resistance of a composite sample and a noncomposite sample (of equal wall thickness), consider the following dimensions and thermal conductivities of a sample:

$\Delta L = 4.0$ in.

$r_1 = 0.368$ in.

$r_2 = 0.407$ in.

$r_3 = 0.462$ in.

$r_4 = 0.502$ in.

$K_1 = K_3 = 12.14$ Btu/hr·ft·°F (at 500°C)[13]

$K_2 = 207$ Btu/hr·ft·°F (at 500°C)[14]

The calculated thermal resistance of the composite (R_C) and stainless steel (R_{SS}) were found to be respectively 0.007108 and 0.012266 hr·°F/Btu, indicating the thermal resistance of the composite to be appreciably lower. If thermal contact resistance exists at the stainless steel/copper interface, then one can modify Eq. 3 by taking these additional resistances into account as follows:

$$Q = \frac{\Delta T}{R_1 + R_{1-2} + R_2 + R_{2-3} + R_3} \quad \ldots \tag{4}$$

where R_{1-2} and R_{2-3} are the interfacial thermal resistances, defined as

$$R_{1-2} = \frac{\Delta T_{1-2}}{Q} \; ; \; R_{2-3} = \frac{\Delta T_{2-3}}{Q} \quad \ldots \tag{5}$$

where ΔT_{1-2} and ΔT_{2-3} are the temperature drop across the interfaces. An experimental program was undertaken to measure the interfacial thermal resistances ($R_{1-2} + R_{2-3}$) for a sample of SS/Cu/SS composite, as described above.

The thermal conductivity of a sample of Type 304 stainless steel, in the form of a hollow cylinder (1-in. OD, 0.75-in. ID, and 4 in. long), was measured by the guard heater principle. The purpose of this experiment was to check out assembly and instrumentation procedures using a sample of known thermal conductivity before determining the interfacial thermal resistances of selected metal composites.

Figure 8 shows schematically the assembly of the sample and the guards. The sample and the guards are heated from within by means of 0.5-in.-dia by 4-in.-long cartridge heaters. Chromel-alumel thermocouples are spot-welded to the inner and the outer walls of the sample and the guards (see Fig. 8). By connecting A_3 to A_{10}, A_4 to A_{11}, and so on, differentially, the temperature drop across the metal walls can be measured directly. The thermocouples A_{11}, B_{11} and C_{11}, with appropriate reference junction, measure the absolute temperature at which thermal conductivity measurements are being made. Differential thermocouples A_5-B_3 and A_{12}-B_{10} measure the axial temperature

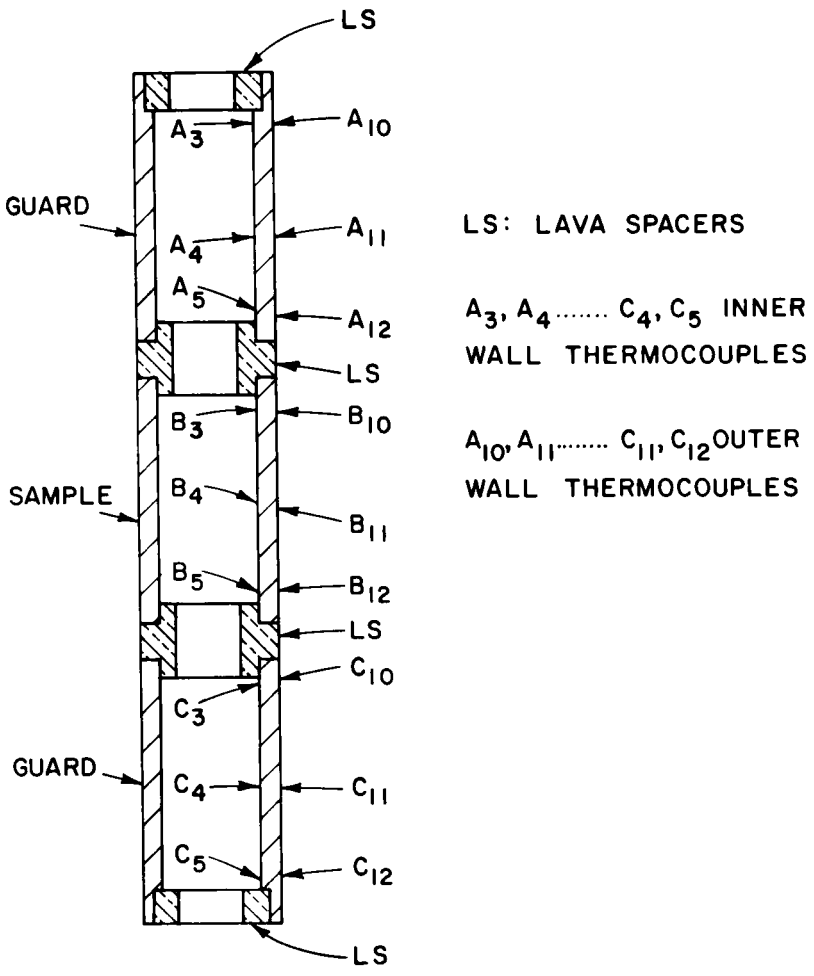

Fig. 8. Thermocouple Locations

gradients between the sample and the guard. Figure 9 shows the heater arrangement and instrumentation used to measure the heat input to the sample. By adjusting heaters A and C (guard heaters), the axial temperature gradients, as indicated by the differential thermocouple A_5-B_3 or A_{12}-B_{10} (and similar differential couples for heater C), can be reduced to very near zero. Thus, the heat input to the sample by heater B flows in the radial direction only.

The current flow through the sample heater is measured by a calibrated shunt. The potential drop across the heater is measured by a voltage divider, using precision resistors. The potential drop across the shunt and the voltage divider are measured by a digital voltmeter with an accuracy of ±2 μV. The digital voltmeter was also used to measure all the differential and absolute temperatures (with the ice point as the reference cold junction).

Table 1 compares the measured thermal conductivity values for the stainless steel with the published data.[13] The thermal conductivity values at 770 and 1049°F compare favorably with the published data. However, the

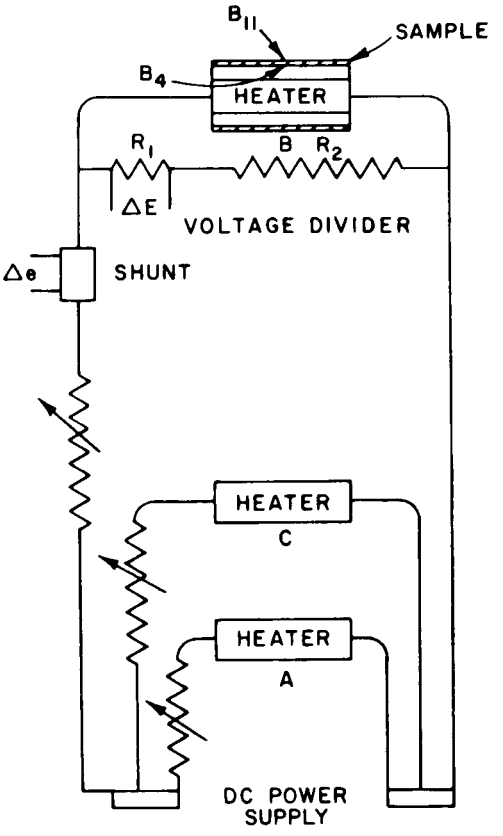

Fig. 9. Instrumentation for Sample Heating

Table 1. Thermal Conductivity of Type 304 Stainless Steel

	K_m, Btu/hr·ft·°F	
Temperature, °F	Measured	Published
445	5.61	10.1
770	10.05	11.3
1049	12.13	12.6

low-temperature value is in error. One of the reasons for this discrepancy may be the error associated with measuring the very small temperature differential observed in this case (less than 1°F), using chromel-alumel thermocouples.

Next, the measurements were carried out for the stainless steel/copper/stainless steel composite sample with identical dimensions and essentially identical instrumentations. The results are summarized in Table 2.

Table 2. Thermal Conductivity of Stainless Steel/Copper/Stainless Steel Composite

Temperature, °F	K_m, Btu/hr·ft·°F
402	4.11
585	4.03
810	3.35
1020	3.33

In view of the fact that the composite layers do not make perfect contact with each other, and that a gap was found to exist between the layers before the sample was heated, the low values of the initial thermal conductivities given above were not unexpected. It is also expected that these values would get progressively lower as heating of the sample in air continued at temperatures higher than 500°F, where oxidation of both the copper and stainless steel layers occurs. After keeping the sample at about 1000°F for 24 hr, the sample was cooled to room temperature and the tests were repeated. The results are given in Table 3.

Table 3. Thermal Conductivity of Composite after Prolonged Heating.[a]

Temperature, °F	K_m, Btu/hr·ft·°F
450	1.61
560	0.49
814	0.40
1023	0.33
462 (repeat)	0.48

[a]Sample heated at 1000°F for 24 hr prior to second test.

The additional reduction in the thermal conductivity values indicated by these data is attributed to oxidation of the metallic surfaces.

III. ASSESSMENT OF THE TRITIUM CONTAINMENT AND PROCESSING REQUIREMENTS FOR EXPERIMENTAL FUSION DEVICES

(B. Misra and V. A. Maroni)

During the past year, members of the Fusion Reactor Research Group in the Chemical Engineering Division have participated in laboratory-wide design studies of two experimental fusion devices: a Tokamak experimental power reactor (ANL/EPR)[15] and a Tokamak engineering technology facility (ANL/TETF).[16] In addition, a fairly comprehensive analysis of hydrogen isotope enrichment scenarios for various types of fusion reactor concepts has been completed. Summaries of the design studies for the tritium-handling systems on ANL/EPR and ANL/TETF and results of the enrichment analyses are given below.

A. Summary of the ANL/EPR Tritium Facility Design

The ANL/EPR tritium-handling system must separate tritium and deuterium from the spent fuel and must be capable of cleaning up the atmosphere in the building in the event of a large tritium release. The key operating parameters of the system are given in Table 4, and a schematic of the system is shown in Fig. 10. The principal assumptions applied in determining these parameters are as follows: (1) the throughput/burnup ratio will be approximately 50; (2) the fuel cycle turnaround time (fuel holdup time) will be four hours or less; and (3) the initial tritium inventory of $\leq$1.5 kg will be supplemented as needed (from an outside production facility) to match the burnup encountered during operation. The fuel cycle turnaround time is determined mainly by the regeneration cycle of the cryosorption pumping system for the toroidal plasma chamber. The present plan is to carry out this regeneration cycle on a 4-hr basis.

Analysis of the cleanup requirements following a massive release of tritium ($\leq$100 g) to the reactor hall has resulted in the definition of an atmospheric detritiation procedure. The volume of the reactor hall is $\sim 2.8 \times 10^5$ m^3 ($\sim 10^7$ ft^3), and the assumption has been made that the normal operating level of tritium in the hall atmosphere (air) will be maintained at the recommended MPC level for workers, 5 μCi/m^3. Provision is made to handle a release that would result in a $\leq 10^6$ increase in the tritium activity in the reactor hall atmosphere. This is based on the assumption that the escape of 100 g of tritium represents the largest credible event that could occur in the reactor building without a simultaneous breach in the building containment boundaries. The cleanup is to be completed within two days, using a catalyst system operating at room temperature. Key parameters for this system are listed in Table 5.

Calculations have been made to estimate the rate of tritium permeation from the plasma chamber into the first-wall cooling-water circuit. These calculations show that the tritium level in the first-wall cooling water ($\sim 10^5$ liters) increases to a maximum of $\sim$1 Ci/liter after one year. The handling practices associated with this pressurized cooling water would be essentially the same as those currently applied to the pressurized D_2O primary circuits of heavy water reactors that commonly run up to 10 Ci/liter.

Potential off-site tritium exposure calculations have been made. Two events leading to off-site exposure due to the release of tritium have been considered. The first event considers 2% ($\sim 4 \times 10^5$ Ci) of a total inventory

Table 4. Summary of Tritium-Handling System Parameters

	B_{max}^{TFC}[a]	
	8 T	10 T
General		
Power during burn, MW	200	500
Burn-cycle duty cycle, %	75	75
Plant availability factor, %	67	67
Tritium burnup, g/day	26	64
Throughput/burnup ratio	50	50
Tritium delivery rate, g/hr	60	150
Fuel cycle turnaround time, hr	4	4
Plant inventory, kg	0.6	1.5
Annual tritium consumption at 50% capacity factor, kg	6.4	16
Tritium Inventory Disposition		
Cryosorption pumps, g	240[b]	600[b]
Getter beds, g	240[b]	600[b]
Distillation columns, g	10[b]	25[b]
Fuel cycle hardware, g	10[b]	25[b]
Storage, g	∿500[b]	∿1300[b]
Anticipated mean inventory, g	600	1500
Fuel Cycle		
Nature of fuel processing and recycle systems	Nonmetallic element removal Debris removal Isotopic enrichment Fuel storage Fuel delivery	
Type of mainstream enrichment	Cryogenic distillation	
No. of columns	6	
No. of equilibrators	1	

[a] Maximum value of the toroidal field.

[b] Maximum value at any single time.

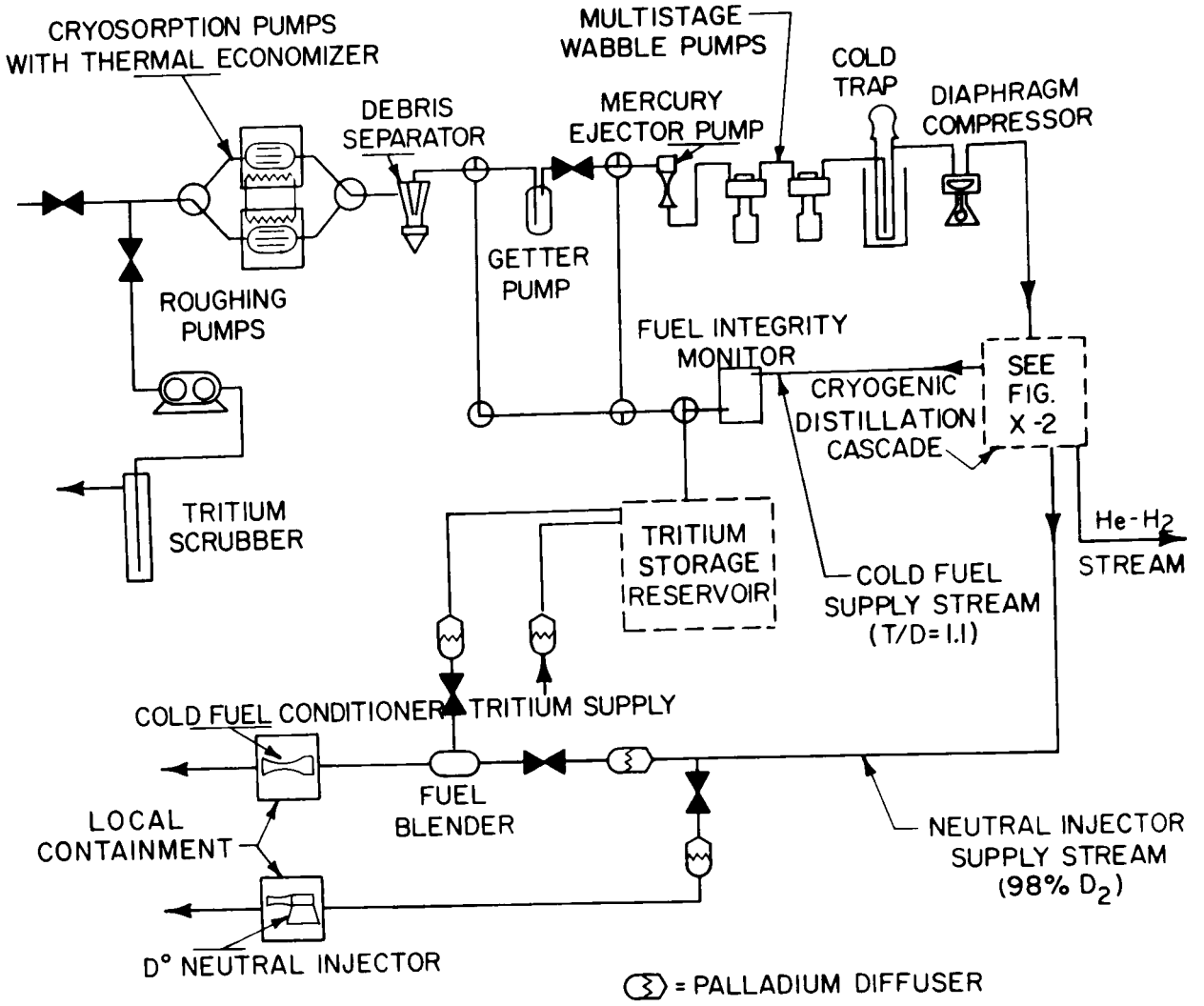

Fig. 10. Fuel Cycle Schematic for the ANL/EPR

Table 5. Atmospheric Cleanup System

Reactor hall volume (m^3)	$\sim 2.8 \times 10^5$
Baseline tritium level ($\mu Ci/m^3$)	5
Cleanup time (days)	≤ 2
Maximum decontamination factor	10^6
Air circulation rate (emergency) (cfm)	$\geq 10^5$
Volume of catalyst (m^3)	20
Catalyst operating temperature (°C)	27

of 2 kg of tritium released at ground level as water vapor in an accident. The dose commitment for an individual at the site boundary is 23.5 rem (whole body) at 500 m and 7.4 rem (whole body) at 1000 m as compared to the 10 CFR 100 guideline for total body dose of 25 rem. The second event is the continuous daily release of 100 Ci of tritium, for which the concentration at 500 m is $\sim 5 \times 10^{-9}$ Ci/m^3 and at 1000 m is $\sim 2 \times 10^{-9}$ Ci/m^3. ERDA Manual 0524 gives the uncontrolled concentrations guide as $\leq 2 \times 10^{-7}$ Ci/m^3.

B. Tritium Processing and Containment for the ANL/TETF

Essentially all of the tritium entering the torus of the TETF during operation is delivered by the T^0 neutral injectors. Maintaining a feed rate to the torus of $\sim$15 g/hr requires that $\sim$120 g/hr be supplied to the T^0 neutral injection system. Coupling these feed rates with other considerations related to injector pump turnaround times, processor holdups, and reserve storage requirements has led to an estimated tritium inventory for the TETF of $\sim$650 g. The operating scenario conceived for TETF fuel recycle and processing is based on four T^0 neutral injectors, each equipped with two interchangeable gas-pumping systems that are regenerated on an hourly basis. The tritium inventory within each injector is cleaned up twice a day by one of three parallel exhaust-processing systems. Pumping and processing for the four D^0 neutral injectors are carried out in essentially the same manner as described above for the T^0 injection systems. The plasma exhaust is processed by a separate system and is turned around once a day. Each of the three processing systems (for the T^0 injectors, D^0 injectors, and the plasma exhaust) contains (1) a purification train to remove nonhydrogenous impurities and (2) a cryogenic distillation cascade to carry out the required hydrogen isotope separations. Characteristics of the tritium systems are summarized in Table 6.

Table 6. TETF Tritium System Characteristics

Injection system requirements	
T^0 injection rate to plasma	15 g/hr
T^0 input rate to injectors	120 g/hr
Tritium inventory per injector	15 g
Inventory disposition	
Injector systems (4)	120 g
Processors for injector recycle (3)	45 g
Plasma exhaust and processing system (2)	360 g
Contingency reserve storage (1)	120 g
Total	$\sim$650 g
Tritium consumption rate	880 g/yr
Tritium accumulation in first wall H_2O coolant after 1 year of operation	10^3-10^4 Ci

Fuel would be stored in a concrete-barricaded vault, housing several independently controlled getter-type storage units. The valves, pumps, compressors, monitors, and other ancillary components needed for tritium transfer and control operations require only modest development beyond current state-of-the-art hardware.

Selected considerations of safety implications and environmental impacts related to tritium handling in the TETF indicated that the following occurrences can all be handled within the limitations of current practices and guidelines: (1) tritium accumulation in the first-wall cooling-water circuit, (2) a large accidental release amounting to several percent of the total tritium inventory, and (3) a release rate of 100 Ci/day during normal operation.

With the exception of several difficult problems associated with the T^0 injector systems, most of the tritium-handling and tritium-containment technology required for operation of the TETF appears to be directly applicable or extrapolative to EPRs and other follow-up devices.

C. Enrichment of Isotopes of Hydrogen by Cryogenic Distillation

The estimated fuel burnup during a typical fueling cycle for presently conceived Tokamak-type D-T fusion reactors is only a few percent of the injected species (an equimolar mixture of D and T); hence, based on economic considerations alone, it is essential that the spent fuel mixture by recycled. However, the contaminants produced in the plasma chamber (by such means as sputtering, transmutation, permeation, and chemical reaction) must be removed from the spent fuel mixture before the fuel can be reinjected. While removal of contaminant atoms of high molecular weight appears to present no serious problem, the purification of the hydrogen isotopes (H_2, HD, HT, D_2, DT and T_2) into reinjectable forms is a formidable task. Not only must the protium atoms be removed from the fuel "ash", but the tritium and deuterium atom fractions must be properly adjusted for both cold fuel and neutral beam reinjection. Of the several enrichment schemes under consideration, isotope separation by cryogenic distillation appears to be the most promising. An examination of the composition of the spent gases and the purity and composition of the injected fuel shows that a relatively complex separation scheme involving upwards of six distillation columns, arranged in cascade, would be needed. Before a complex enrichment scheme can be adequately analyzed, the basic computational tools must be developed. The following summary presents (1) mathematical formulation for the analysis of equilibrium stage distillation processes, together with solution of the resultant equations using the IBM System 370/195, and (2) the application of the computer program in analyzing the enrichment processes for two distinctly different fuel cycles.

1. Description of the Calculational Method

A variety of analytical techniques[17-19] have been used in the design of multicomponent distillation columns. While most of these methods are adequate to fulfill the needs of the chemical process industries, only the exact method of solution by matrix algorithm appears suitable for isotope separation. The inaccuracies inherent in empirical schemes and trial-and-error solutions make these methods largely unsuitable for achieving the level

of accuracy required in the analysis of isotopic fuels. Hence, at the outset, it was decided to proceed with analyses based on an exact method of solution of the governing equations to insure that the accuracy of the analytical results would be limited only by the accuracy of the thermodynamic and phase equilibrium data.

A complex distillation column may contain many feeds, side streams, and other special features. The feed compositions may vary widely and may be introduced at any stage (or plate) (see Fig. 11). Several simplifying

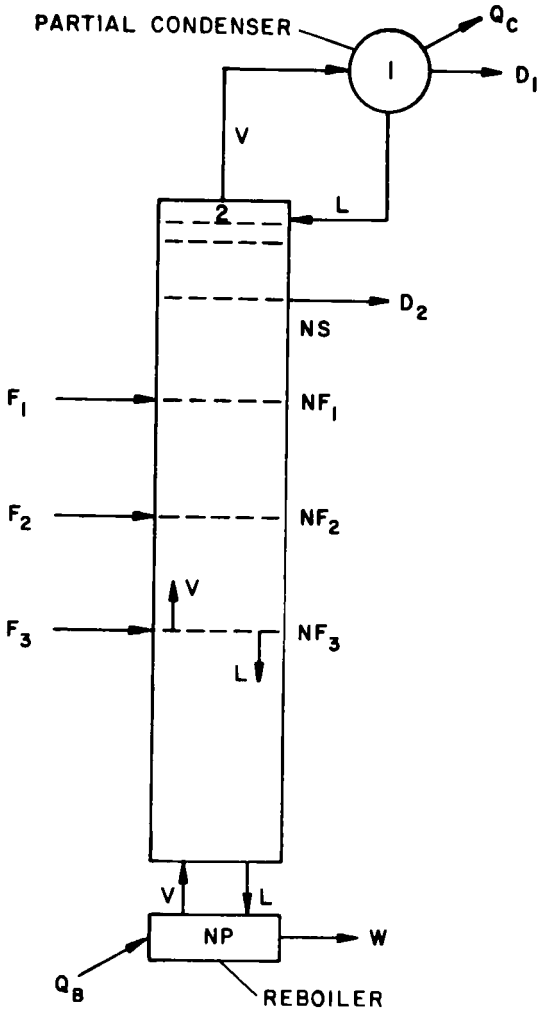

Fig. 11. Schematic of Complex Distillation Column

assumptions, of necessity, were made before the development of the mathematical model was carried out. The ideal equilibrium stage concept, in conjunction with the laws of conservation of mass and energy, was utilized to describe the functional relations among the various components, which are assumed to form ideal mixtures.

The composition of the feeds, and the rates of the feeds, the distillate, and the side streams are assumed to be known. For a given number of equilibrium or theoretical stages (NP), assumed feedplate (NF_1, NF_2, NF_3) and side stream (NS) locations, and reflux ratio (L/D), the functional relationship between the various components across the distillation column may be expressed mathematically. For component i, of a total of NC components, the law of conservation of mass and phase equilibrium leads to NP equations, each containing NP terms, which may be expressed in matrix algebra as follows:

$$AX = B \tag{6}$$

where

A = NP x NP	coefficient matrix
X = NP x 1	solution vectors
B = NP x 1	column vectors

The nature of the physical problem is such that it leads directly to the tridiagonal matrix represented by Eq. 6. It should be noted that there are NC sets of independent equations (one for each component) of the type represented by matrix Eq. 6. For a physical problem, since the determinant of the NP x NP square matrix is nonsingular, the solution of Eq. 6 is given by

$$X = A^{-1}B \tag{7}$$

where A^{-1} is the inverse of matrix A. Hence, the solution of Eq. 6 results in NP values of component i, one value corresponding to each equilibrium stage. Similarly, the solution of the remaining sets of the Eq. 6 type gives the mole fractions of the other components in the liquid mixture. Thus, the mole fractions of all components at each equilibrium stage are determined simultaneously.

The correct solution is obtained when the following criterion is satisfied (with an acceptable degree of tolerance) *simultaneously at each stage:*

$$\sum_{1}^{NC} y_i = 1 = \sum_{1}^{NC} k_i x_i \tag{8}$$

where x_i, y_i, and k_i are, respectively, liquid mole fraction, vapor mole fraction, and equilibrium constant for component i. Existing vapor pressure data[20] for six hydrogen isotopomers were used to calculate the equilibrium constants.

A detailed description of the main computer code, including FORTRAN listings, the supporting subroutines, and data input and output options, is given in Ref. 21. The versatility of the computer code may be demonstrated by analysis of a number of cases as summarized below.

In order to study how enrichment of the spent fuel proceeds across a distillation column, a number of simplified cases, with only a single feed and no side stream draw-off, were analyzed. The composition of the feed (spent fuel) was assumed to be representative of the presently conceived

Tokamak-type reactor such as the ANL Experimental Power Reactor (ANL/EPR). Several cases were analyzed by varying the number of theoretical stages, reflux ratio, feed-plate location, and operating pressure in order to (1) study the behavior of distillation columns handling isotopes of hydrogen, and (2) detect any anomalous behavior of the computer code such as failure to converge. Some of these results are summarized in Table 7.

2. Cryogenic Enrichment Scenario for the ANL/EPR

Before an enrichment scheme for the EPR can be developed, the composition of the spent fuels and the purity requirements of the reinjectable fuels must be established. The composition of the spent gases, as given below, may be considered as representative of a typical experimental power reactor such as ANL/EPR.

Protium (at. %)	2.1
Deuterium (at. %)	48.95
Tritium (at. %)	48.95

For the presently conceived fuel-injection scheme, the following are some of the requirements for the light and the heavy fraction:

(1) The lightest fraction should contain all of the protium atoms, with as little tritium as possible so that this fraction can (if necessary) be sent to waste consolidation and burial without further reprocessing.

(2) One of the heavy fractions must contain >98 at. % deuterium so that it may serve as the fuel for the neutral beam injector.

(3) The composition of the other heavy fraction should be such that the ratio of tritium to deuterium atoms is approximately 1.1 so that the fuel composition resulting from cold fuel and neutral injection has $T/D \simeq 1.0$.

An examination of the feed composition and reinjection requirements, as listed above, shows that several distillation columns operating in cascade would be required. Figure 12 shows the 6-column cascade developed for the ANL/EPR. The analytical results are summarized in Table 8.

An examination of the bottom products from columns No. 1 and 6 shows that the composition of these two feed mixtures essentially meets requirements (2) and (3) above. However, the distillate from column No. 4 cannot be directly discharged for waste consolidation and burial without further reprocessing because of its high tritium content.

An attempt was made to reduce the tritium content in the distillate from column No. 4 by varying the number of theoretical stages, reflux ratio, and operating pressure. The tritium content could not be returned to acceptable levels owing to the presence of tritium as HT, which is relatively volatile. Hence, all of the protium atoms cannot be removed easily by distillation alone, without carryover of some tritium atoms.

Table 7. Summary of Operating Parameters and Analytical Results of Cryogenic Enrichment for ANL/EPR[a]

Parameter	Column Pressure, torr	No. of Plates	Feed Plate Location	Reflux Ratio	Top Product, at. %			Bottom Product, at. %		
					H	D	T	H	D	T
Effect of Reflux Ratio	1000	30	15	5	6.8	72.4	20.8	0.08	38.9	61.0
				10	7.0	80.0	13.0	0.02	35.6	64.3
				15	7.0	83.2	9.8	∿0	34.4	65.6
				20	7.0	84.7	8.3	∿0	33.8	66.2
				25	7.0	85.5	7.5	∿0	33.4	66.6
Effect of Feed Plate			10	15	7.0	81.7	11.3	∿0	35.0	65.0
			15		7.0	83.2	9.8	∿0	34.7	65.3
			20		7.0	83.0	10.0	0.02	34.4	65.5
Effect of No. of Plates		25	12		7.0	81.1	11.9	0.01	35.2	64.8
		20	10		6.9	78.7	14.4	0.02	36.2	63.8
		15	8		6.9	75.4	17.7	0.06	37.6	62.3
Effect of Pressure	500	30	15	15	7.0	86.2	6.8	∿0	32.6	67.4
	1000				7.0	83.2	9.8	∿0	34.3	65.6
	1500				7.0	81.0	12.0	∿0.01	35.3	64.7
	2000				7.0	79.4	13.6	∿0.02	36.0	64.0
	2500				6.9	78.1	15.0	∿0.03	36.5	63.4

[a]Input composition = 2.10% H, 48.95% D, and 48.95% T.

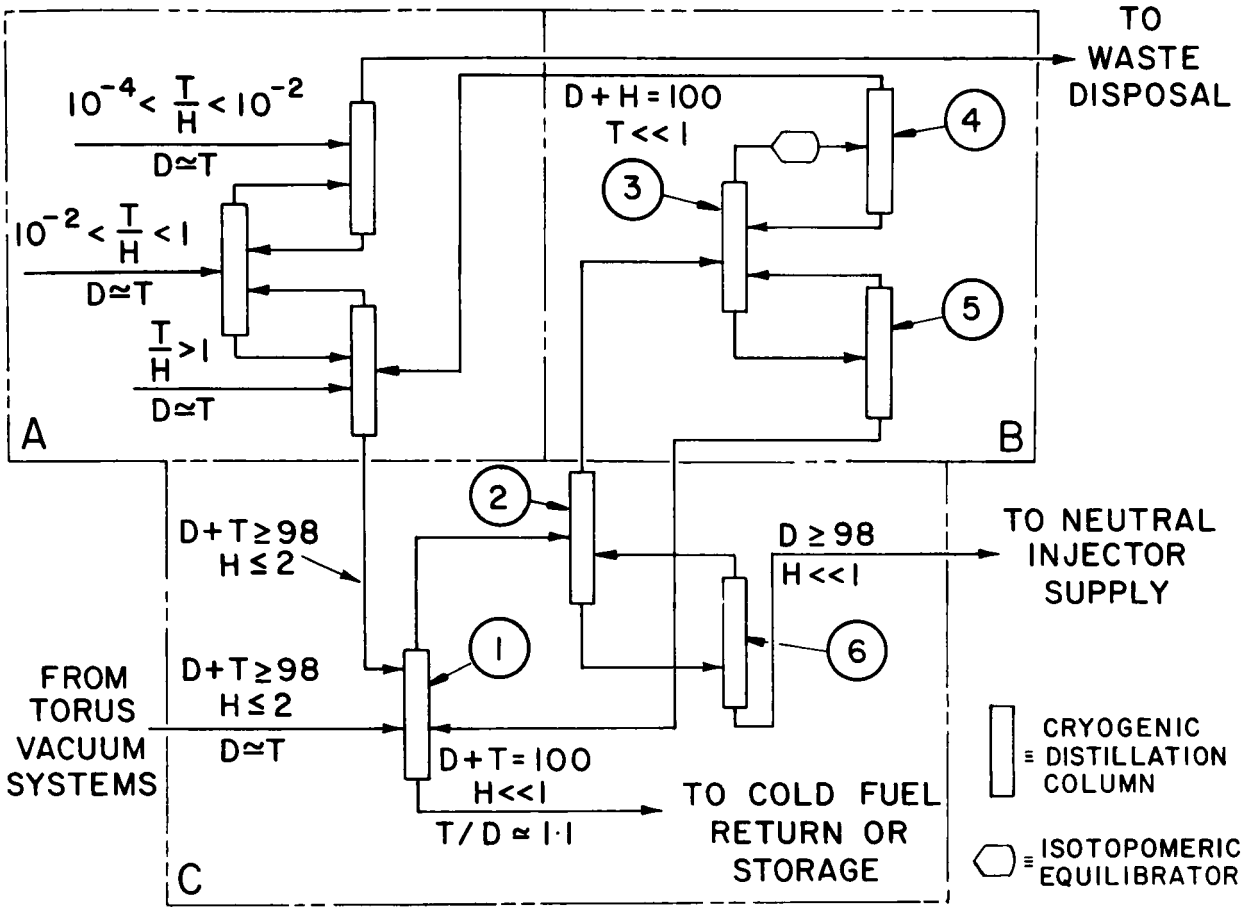

Fig. 12. Cryogenic Enrichment Scheme for ANL/EPR

The isotopomeric composition of the equilibrium feed mixture that distills from the top of column No. 3 can be altered by shifting the equilibrium among the various molecular hydrogen species by passing the mixtures through a chemical equilibrator, with or without addition of excess deuterium. The effect of a chemical equilibrator can be seen from the results shown in Table 8.

3. Cryogenic Enrichment Scenario for More Stringent Enrichment Requirements

Based on the studies presented in this report, it is apparent that the enrichment requirements of a fusion device are largely determined by the composition requirements of the fuel supply stream(s). It is also a reasonable assumption that most D-T-burning experimental reactors (Tokamaks or others) will produce an exhaust-system composition that is not significantly different from the one used above for the ANL/EPR. In order to extend the cryogenic distillation analyses to a machine with more stringent mainstream enrichment requirements than the EPR, the case of a fully-injected Tokamak reactor was considered. The previously described Tokamak engineering

Table 8. Summary of Operating Parameters for the ANL/EPR Cryogenic Distillation Cascade

Column Number[b]	Feed Plate	Total Feed, mole	Feed Composition, at.%			Top Product				Bottom Product			
						Total Moles	at. %			Total Moles	at. %		
			H	D	T		H	D	T		H	D	T
1	10 15 20	100	4.12	49.57	46.31	18	21.9	63.0	15.1	82	0.2	46.6	53.2
2	15 20	23	17.35	70.57	12.08	13	30.3	50.0	19.7	10	0.5	97.3	2.2
3	10 15 20	23	38.51	34.86	26.63	8	50.9	31.1	18.0	15	31.9	36.9	31.2
4	15	8	50.9	31.1	18.0	3	53.0	45.9	1.1	5	49.7	22.3	28.0
5	15	15	31.9	36.9	31.2	5	48.7	4.6	46.7	10	23.5	53.0	23.5
6	15	15	0.5	97.3	21.7	5	1.0	97.9	1.1	5	0	96.7	3.3
4[c]	15	8	50.8	29.2	20.0	3	96.1	4.5	0	5	22.2	44.8	32.7

[a] 30 theoretical stages per column; column pressure 1000 torr, except for column No. 1 operating at 500 torr

[b]

technology facility (TETF) was used as a point of departure for this analysis, because the TETF has the requirement that all deuterium and tritium atoms are delivered to the plasma chamber in the form of isotopically separated energetic neutral particle beams. The exhaust stream composition was taken to be 0.2 at. % H_2, 0.8 at. % HD, 0.8 at. % HT, 27.7 at. % D_2, 42.8 at. % DT, and 27.7 at. % T_2.

Since the D_2 and T_2 fractions represent less than 56% of the exhaust stream, complete recycling of the spent fuel cannot be carried out by cryogenic distillation alone. The other requirement, as for ANL/EPR, is to remove most of the protium atoms without carryover of significant quantities of tritium atoms. To fulfill the above reinjection requirements (separate streams of >95% D_2 and >95% T_2), an enrichment scheme consisting of five distillation columns and two equilibrations was derived for the TETF-type device (see Fig. 13). The analytical results are shown in Table 9.

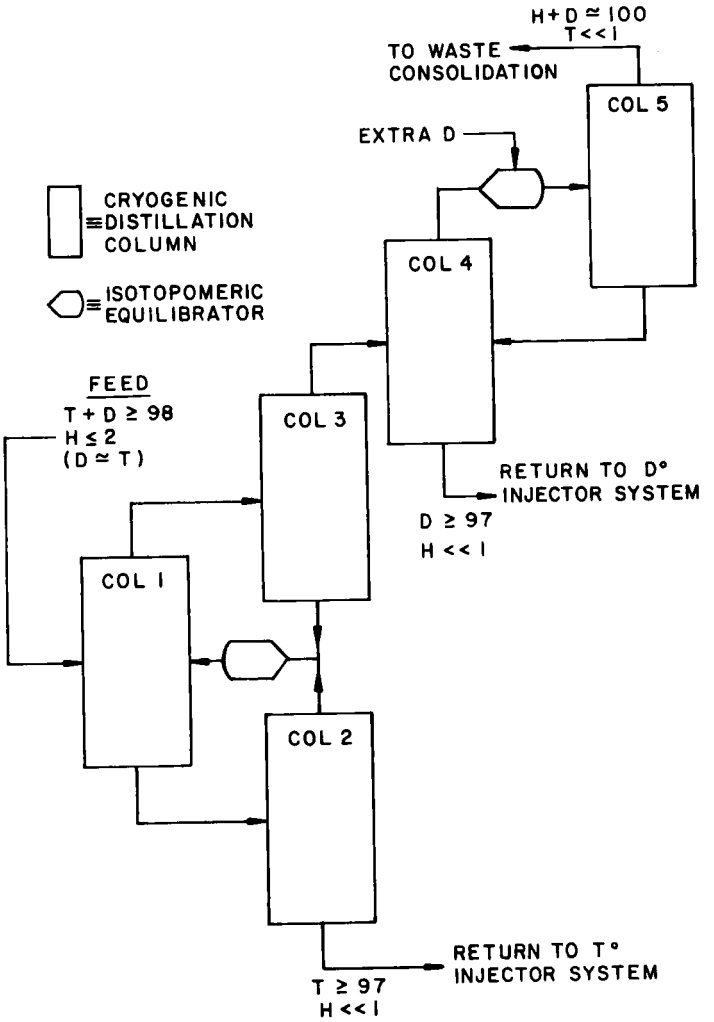

Fig. 13. Cryogenic Enrichment Scheme for TETF

Table 9. Summary of Operating Parameters for the TETF Cryogenic Distillation Cascade[a]

Column Number[b]	Feed Plate	Total Feed, mole	Feed Composition, at. %			Top Product				Bottom Product			
						Total Moles	at. %			Total Moles	at. %		
			H	D	T		H	D	T		H	D	T
1	15 20	100	0.49	49.64	49.87	50	1.0	74.9	24.1	50	0	24.4	75.6
2	15	50	0	24.4	75.6	27	0	42.5	57.5	23	0	3.2	96.8
3	15	50	1.0	74.9	24.1	25	2.0	93.9	4.1	25	0	55.9	44.1
4	15 20	28	1.77	94.51	3.72	5	9.4	87.1	3.5	23	0.1	96.1	3.8
5	15	5	9.4	87.0	3.6	2	23.1	68.5	8.4	3	0.2	99.4	0.4
5[c]	15	5.5	8.6	88.2	3.2	2.5	18.8	80.6	0.6	3	0	94.6	5.4

[a] 30 theoretical stages per column; pressure for columns 1, 2, and 3 equal to 1000 torr; pressure for columns 4 and 5 equal to 500 torr.

[b] See Fig. 19 for location in cascade.

[c] After chemical equilibration at 300 K.

4. Conclusions

Mathematical simulation of multicomponent distillation and computer solution of the resultant equations were carried out. Since the computational steps are based on an exact solution method, the accuracy of the analytical results is expected to be limited only by the accuracy of the thermodynamic and phase equilibrium data. Although the computer code was developed specifically for enrichment of the spent fuels from presently conceived Tokamak-type fusion reactors, the scope of this program is much broader in that it can be used in the design and analysis of multicomponent distillation for any liquid mixture, provided, of course, that the necessary thermodynamic and phase equilibrium data are available. The program is very efficient so that a number of parametric investigations to study the effects of design and operating variables can be carried out even with limited resources. The program does, however, require a fairly large computer storage (approximately 250 K bytes).

Using this general purpose computer code as a basis, a distillation cascade consisting of six cryogenic columns was developed and analyzed for the ANL/EPR. The analytical results show that enrichment of the spent fuel sufficient to meet the fuel injection requirements of ANL/EPR can be carried out in a straightforward manner.

Similar analytical studies of spent fuel enrichment for the ANL/TETF show that complete recycling of the fuel for a totally beam-driven device is possible with an enrichment system consisting of only five distillation columns and two chemical equilibrators.

The most important conclusion that may be drawn from the study of the two systems is that, aside from meeting fuel injection requirements, separation of the isotopomeric species of hydrogen can be carried out to any degree of purity by judicious selection of (1) the design and operating parameters (*e.g.*, number of theoretical stages, reflux ratio, operating pressure, etc.) and (2) the number of distillation columns, appropriately interspersed with chemical equilibrators.

IV. DEVELOPMENT OF LIQUID LITHIUM PROCESSING TECHNOLOGY

Starting in FY-1976, the ERDA Division of Controlled Thermonuclear Research has provided support for a program of studies aimed at developing methods of recovering tritium from fusion-reactor blanket materials. Because liquid lithium is a leading candidate for the role of blanket medium in DT-fueled fusion reactors, initial experimental studies have focused on schemes for removing tritium from liquid lithium. For liquid lithium to become a viable fusion-reactor blanket material, it is essential to develop methods of maintaining all nonmetallic elemental impurity concentrations (particularly tritium) at levels of ≤ 1 ppm.[22-24] Studies previously conducted at ANL have shown that this may be possible to achieve by using molten salt extraction as the processing method.[22] Measurements of distribution coefficients between lithium and certain alkali metal halide mixtures have revealed that tritium is preferentially extracted into the salt phase by a factor as high as 4 on a volumetric basis, depending on the salt that is used. These results, in combination with considerations of (1) mutual solubilities between salt and metal, (2) phase separation, (3) blanket neutronics,

(4) corrosion, (5) fabrication, and (6) recovery of tritium from the salt phase, indicate that molten salt extraction of tritium from liquid lithium fusion reactor blankets should be feasible. The most immediate aspect of the molten salt extraction concept in need of verification is the process for removing tritium (present as LiT) from the molten salt after it has been contacted with and separated from the lithium. To this end, experiments are being conducted to evaluate gas-sparging techniques and electrochemical techniques as possible methods of removing deuterium and hydrogen (used as substitutes for tritium) from the extractant salt. In light of the encouraging results obtained to date, the design of a 50-gallon liquid-lithium-processing test loop (LPTL) has been initiated. The purpose of this loop will be to test molten salt extraction and other promising lithium-processing concepts on a reasonable scale. In support of the LPTL design study, a 2-liter capacity mini-test loop has been fabricated and is currently being used to evaluate materials and component performance in advance of construction of the LPTL. Results of efforts in each of the above areas are summarized below.

A. Gas-Sparging Studies
(W. F. Calaway)

Sparging experiments to remove hydrogen isotopes from molten salts have been performed using HCl as the reactive gas and either LiCl-KCl eutectic or a solid solution of LiF-LiCl-LiBr as the molten-salt medium. In the experiment, a quantity of HCl equimolar to the Li plus LiD dissolved in the salt is bubbled through the molten solution, producing the reactions

$$LiD + HCl \rightarrow LiCl + HD \quad (1)$$

$$Li + HCl \rightarrow LiCl + 1/2\ H_2 \quad (2)$$

The lithium metal is introduced to simulate the anticipated conditions of the salt when it returns from the lithium-contacting operation in an actual tritium-processing system. Since hydrogen is only marginally soluble in molten salts, it enters the vapor phase above the salt when liberated by the sparging reactions. The rate and extent of the sparging reactions can be followed by monitoring the hydrogen isotopes in a gas stream above the molten salt.

A schematic drawing of the experimental apparatus for the gas-sparging studies is given in Fig. 14. A stainless steel gas-handling system is connected to a furnace well containing ∿1 kg of salt. Ultra-high-purity argon at ∿800 torr pressure is circulated in a closed loop through the molten salt and past a controlled leak valve that is coupled to a quadrupole mass spectrometer. The system is also equipped with (1) a titanium getter bed (operated at 550°C) that is used to clean the argon sweep gas before and after the experiments and (2) a gas-metering section that permits additions of controlled quantities of sparge gas or hydrogen (for calibration purposes) to the argon stream. To assure optimum gas-liquid interaction, the gas is dispersed throughout the molten salt with either a porous graphite or porous stainless steel bubbler, and the liquid is continuously stirred. The salt-LiD-Li solutions are prepared by weighing out quantities of solid Li and LiD in a helium glove box and transferring these samples to the well in sealed tubes where the samples are dropped directly into the molten salt. A

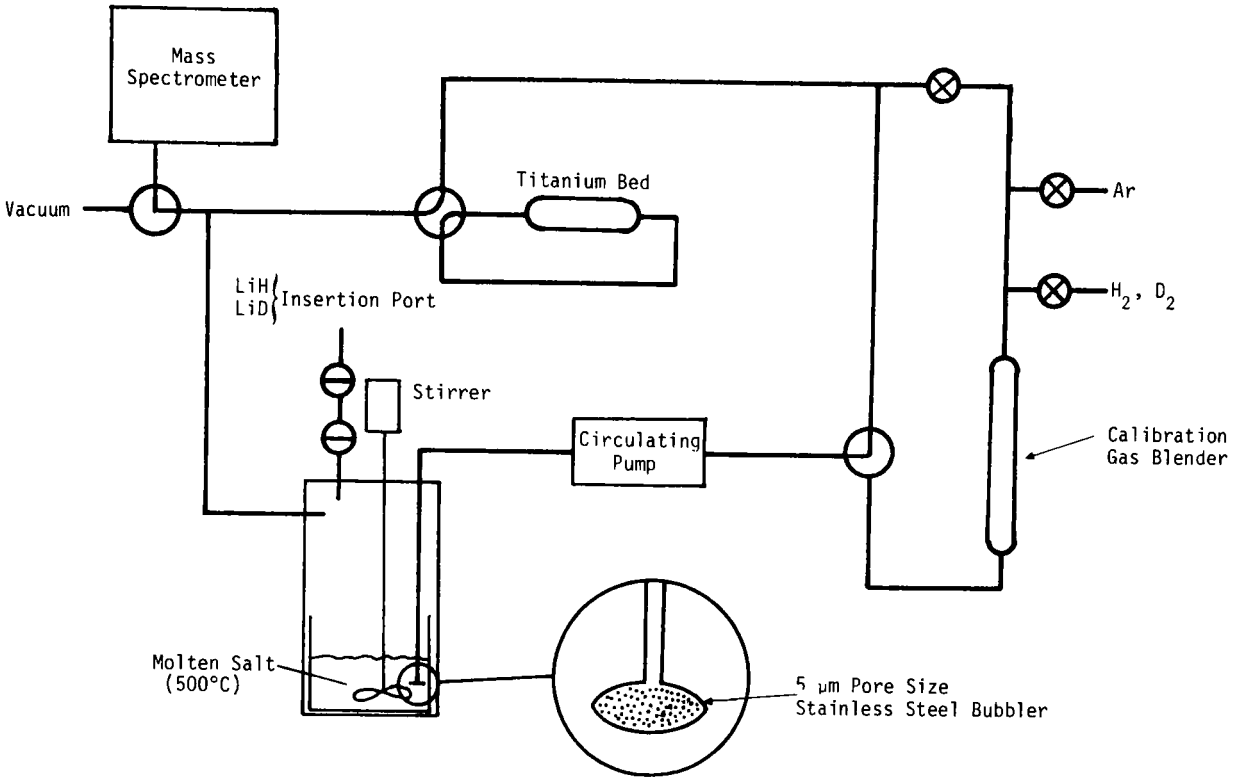

Fig. 14. Schematic Diagram of Apparatus Used for the Gas-Sparging Experiments

double ball-valve arrangement is used as an air lock between the well and sample tubes to assure that air does not contact any of the materials. Hydrogen isotope recovery efficiencies are calculated by comparing the mass-spectrometer peak heights obtained in the experiments with those obtained when known quantities of H_2 and D_2 are circulated in the argon stream.

Initial experiments examined the recovery of LiD from the LiCl-KCl eutectic as a function of such parameters as (1) the concentration of LiD, (2) the concentration of Li, (3) the amount of HCl, and (4) the salt temperature. Results typifying this particular system are given in Fig. 15, where the concentration of HD in the circulating gas stream (as determined mass spectroscopically) is displayed as a function of time. As seen in Fig. 15, and as found in all experiments with LiCl-KCl salt, introduction of LiD caused HD gas to be generated spontaneously. Additional HD was generated by the sparging reaction when HCl was added to the system. Once the reaction had reached completion, the gas stream was directed through the titanium bed which gettered the hydrogen isotopes, and the HD signal returned to its original base line. The spontaneous generation of HD upon addition of LiD was unexpected and was at first attributed to residual HCl or impurities in the system. However, when metallic lithium, which removes impurities and HCl by reaction, was added to the salt, as in Fig. 15, the spontaneous generation of HD persisted. Also typical of these sparging experiments was a low HD recovery efficiency. Generally, less than 50% of the deuterium added to the salt was recovered as HD. For the experiment in Fig. 15, only 38% was recovered.

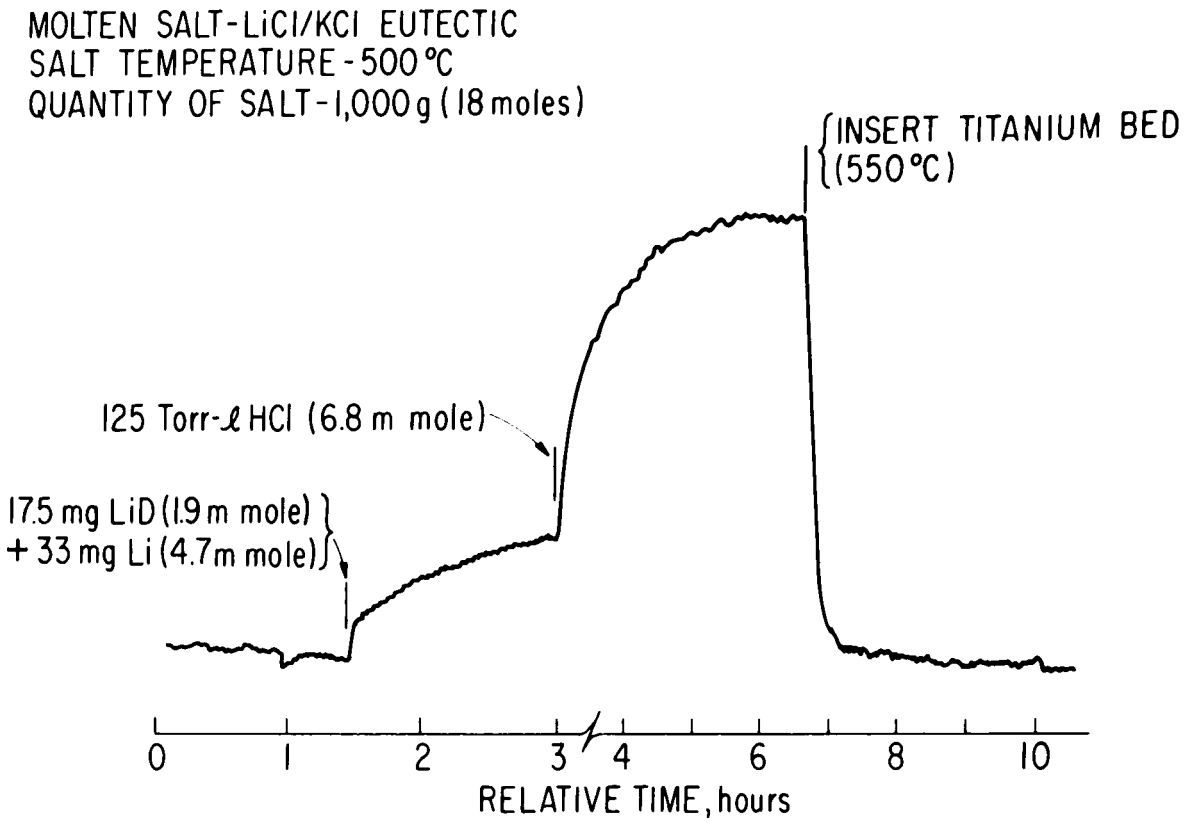

Fig. 15. Results of Gas-Sparging Experiment to Recover 17.5 mg LiD (4 wppm deuteride) from 1 kg of LiCl-KCl

To explore both the spontaneous generation of HD and the poor recovery of HD, experiments were performed in which LiH was extracted from the molten salt with HCl. Results from these experiments revealed the following: (1) recovery of H_2 was significantly improved (compared with HD recoveries), being in the range of 70 to 100% and (2) the amount of H_2 spontaneously generated represented, within experimental error, all of the hydrogen added in the form of LiH: that is, 100% of the hydride added to the molten salt spontaneously converted to H_2. This suggests that D_2 was formed in the LiD experiments and the observed HD was produced as a result of the following exchange reaction:

$$D_2 + H_2 \rightleftarrows 2HD \qquad (3)$$

Treating the molten salt with large quantities of Li or LiH did not appear to slow this spontaneous conversion.

It had previously been recognized that metallic lithium can reduce the potassium cation.[25,26] It may also be true that lithium hydride can reduce potassium cations via the reaction:

$$LiH + KCl \rightleftarrows LiCl + K + 1/2\ H_2 \qquad (4)$$

The potassium generated by the above reaction vaporizes; thus, the salt is a sink for lithium and any hydride in the salt will decompose. The implications of the above reaction do not favor the use of the LiCl-KCl eutectic in any large-scale process because significant amounts of potassium metal would dissolve in the liquid-lithium stream returning to the reactor blanket.

Experiments were, therefore, initiated using a different molten salt, one which did not contain potassium. An all-lithium halide solid solution (9.5% LiF, 22.1% LiCl, and 68.4% LiBr by weight) was prepared and experiments to extract LiH from this salt were performed. Results of one such experiment are given in Fig. 16. Note that spontaneous generation of H_2 did not occur

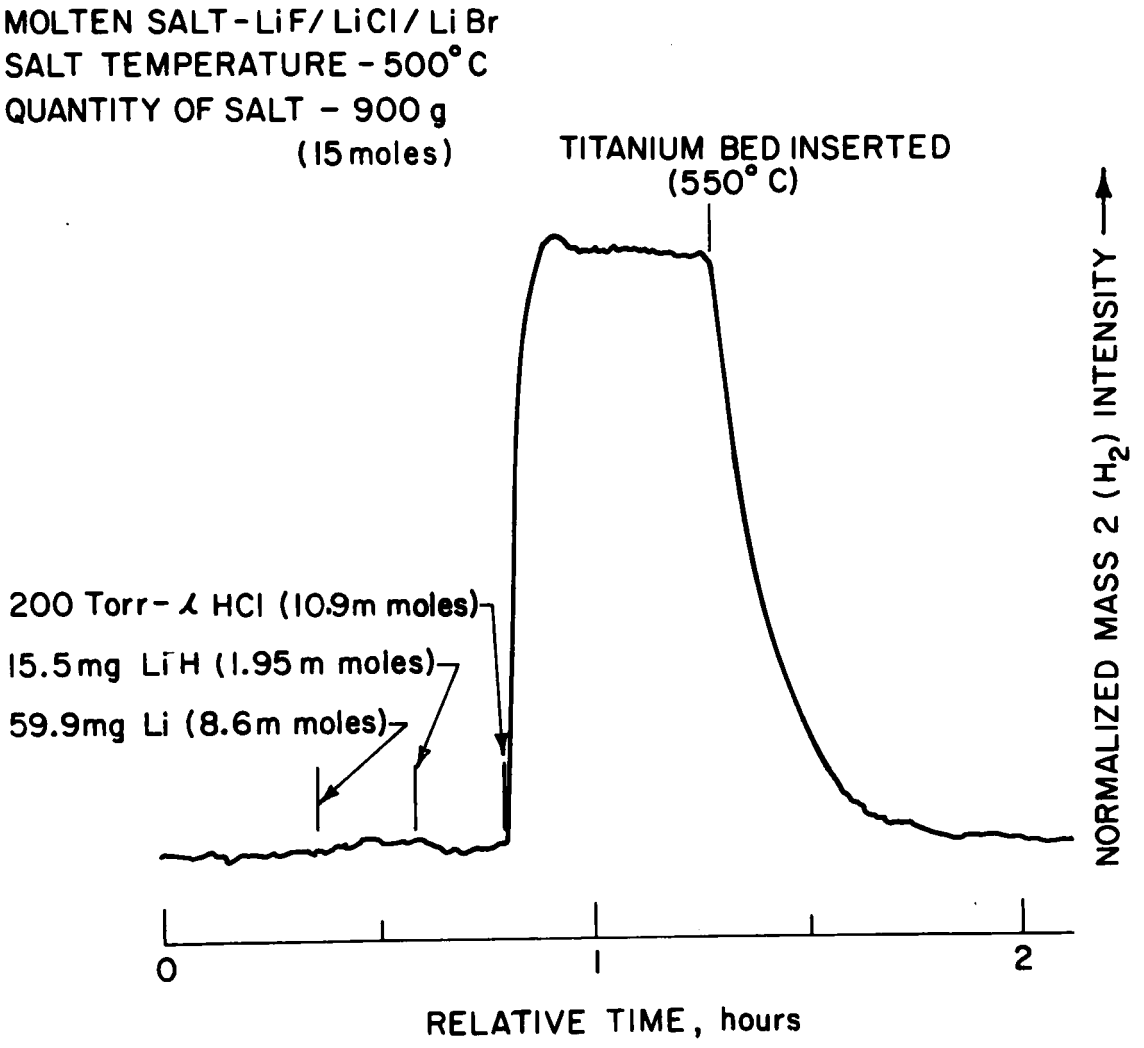

Fig. 16. Results of Gas-Sparging Experiment to Recover 15.5 mg LiH (2 wppm hydride) from 900 g of LiF-LiCl-LiBr

when LiH was added to this salt. The hydride remained in the salt until it was sparged with HCl. The hydrogen gas was then gettered from the stream by the titanium bed. Recovery efficiencies for extraction of LiH from the all-lithium-cation salt were typically in the range of 70 to 100% for hydride concentrations of 5 to 2 wppm. For the experiment shown in Fig. 16, the recovery was 84% of the 2 wppm hydride concentration in the salt.

Using the all-lithium salt, we also examined the extraction of LiD. In these experiments, the three mass peaks of interest (H_2, HD and D_2) were continuously scanned by the mass spectrometer. Results of one such experimen are given in Fig. 17. In the experiment shown, 100 torr-liter of D_2 added to the cover gas was reacted with the lithium added to the salt (not shown in

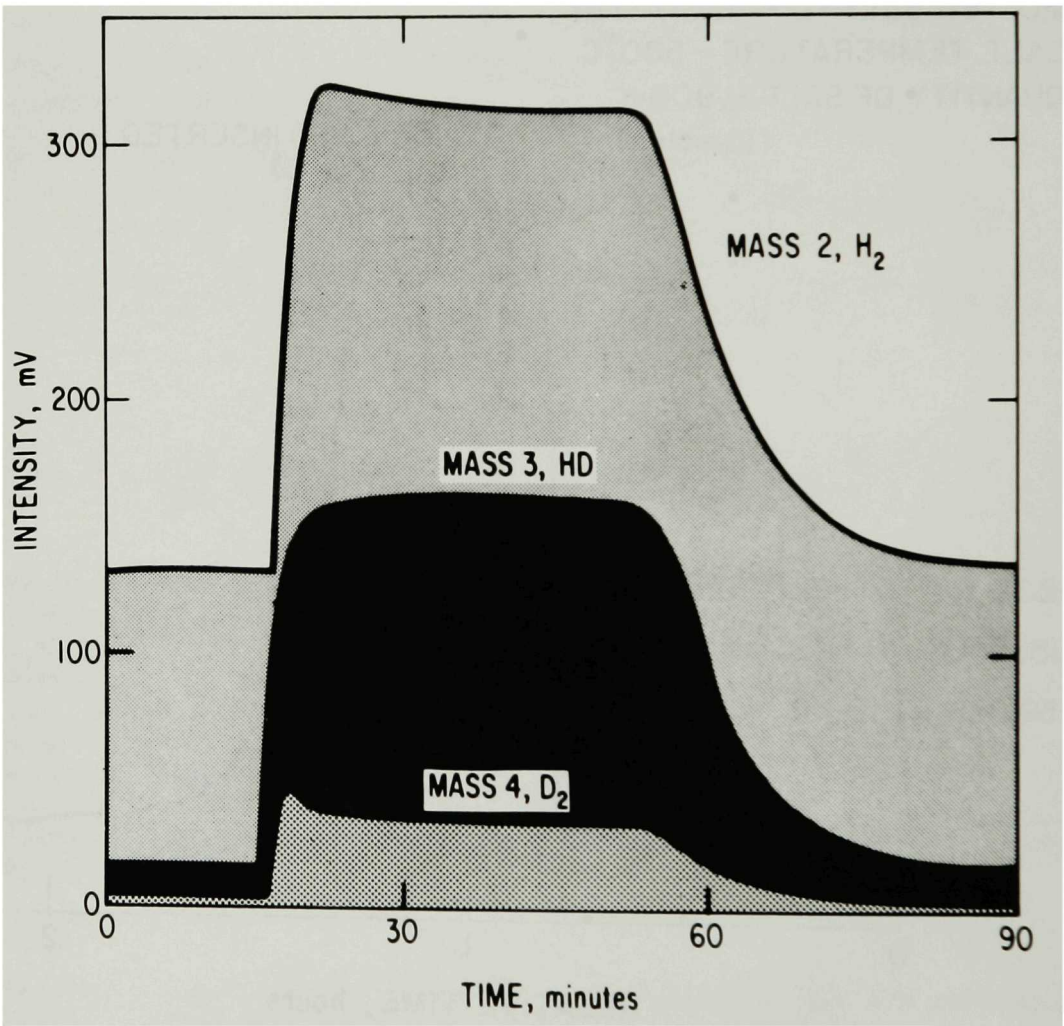

Fig. 17. Recovery of 0.1 g LiD from 900 g LiF-LiCl-LiBr at 500°C. (At t = 15 min, 400 torr-liter of HCl was added to the sparge stream; and at t = 50 min, the gas stream was directed through the titanium bed.)

Fig. 17). The first lithium additions did not lower the D_2 cover-gas concentration, presumably because the lithium reacted with HCl or impurities in the salt. Further additions of lithium reduced the D_2 concentration to background levels. An experiment such as this was unsuccessful when the LiCl-KCl eutectic was used as the molten-salt medium. At time t = 15 min (see Fig. 17), the LiD previously formed was sparged out of the salt with 400 torr-liter of HCl. As is seen, H_2, HD, and D_2 are all generated by the sparging action. The relative heights of the three molecular isotopes confirm that they are equilibrated. The amount of deuterium extracted either as HD or D_2 is 96% of the original amount added to the salt. This represents, within experimental error, total recovery of the deuterium.

The extraction of LiD and LiH from a molten salt (LiF-LiCl-LiBr) by HCl has thus been successfully demonstrated. Removal appears to be complete without adding excess HCl. The complication of having the salt saturated with metallic lithium does not interfere with the extraction process beyond requiring additional amounts of HCl to remove the metal by reaction. In short, gas sparging has proven to be a viable technique for removing hydrogen isotopes from molten salts at the <5 wppm level. With further optimization and refinement of the processing methodology, it is reasonable to expect that the steady-state levels of hydrogen isotopes in the corresponding lithium circuits can be reduced to <1 wppm.

B. Electrochemical Studies

(W. F. Calaway and C. G. Wierdak*)

Experiments are presently under way to develop the methodology for electrochemical extraction of hydrogen isotopes from hydride solutions in molten salts. The advantages of the electrochemical method as compared with the sparging method are (1) reduction of interference from the metallic lithium dissolved in the molten salt and (2) elimination of the need to handle a corrosive sparge gas such as HCl. The experimental apparatus used for these studies is essentially the same as for the sparging experiments. Argon is circulated in a closed loop through molten LiF-LiCl-LiBr while deuterium concentrations in the argon stream are monitored with a mass spectrometer. A hollow porous electrode is used both as the gas bubbler and the anode of the cell so that the D_2 generated by electrolysis is swept out of the salt by the circulating argon before the lithium, which saturates the salt, can back react with the D_2. The cathode is a stainless steel rod. Experiments are performed by applying a constant voltage across the cell and then adding 5 to 10 mg of LiD to the molten salt ($\sim$900 g). Present plans are to test three different types or porous electrodes: (1) a porous graphite electrode, (2) a porous graphite electrode with a ceramic coating,[27] and (3) a porous metal electrode made of sintered 316L stainless steel. To date, both types of graphite electrodes have been examined. Typical results for the uncoated and coated graphite electrodes are given in Figs. 18 and 19, respectively.

When the uncoated graphite electrode is used and the applied potential is at or below 0.8 V, no significant change in either the current through the salt or the D_2 concentration in the argon stream is detected when LiD

---

*Student Aide from Illinois Institute of Technology.

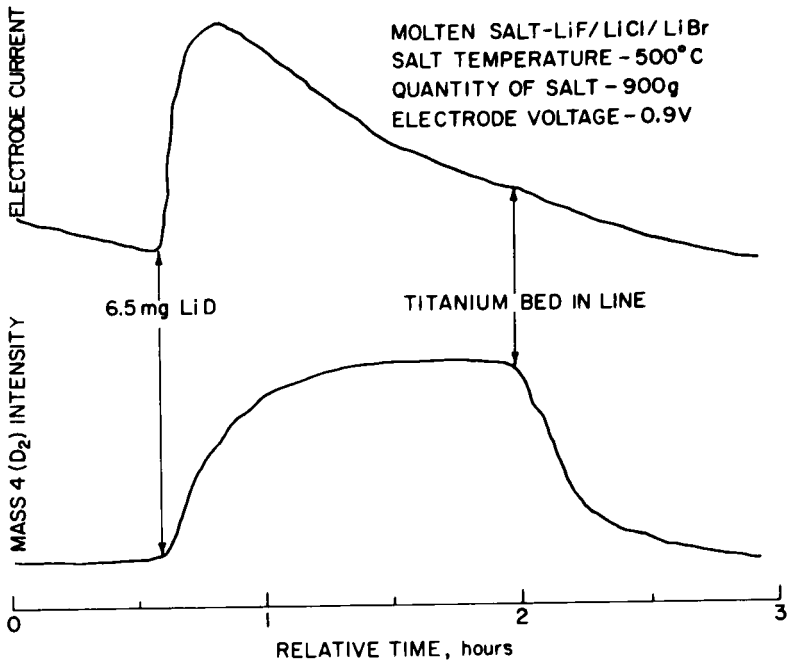

Fig. 18. Results of a Typical Electrochemical Experiment to Evolve Deuterium, Using a Graphite Electrode

crystals are dropped into the molten salt. However, when LiD is added while 0.9 V or more is applied across the electrodes, both the current and the D_2 concentration increase, as shown in Fig. 18. Note that the shapes of both curves are consistent with those expected for the electrochemical evolution process. The current increases sharply when the LiD is added and then decreases as the deuteride ion is depleted from the salt. The D_2 gas concentration increases more slowly and levels off as the electrolysis progresses. Recovery efficiencies (as D_2 and HD) are typically 25 to 50% for these experiments. No buildup of LiD occurred in the salt, which implies that the remainder of the deuterium is being recovered in some other molecular form. This supposition is supported by the observed decrease in recovery efficiency as the electrode potential increases. Two possible mechanisms for the loss of D_2 are (1) decomposition of the salt, allowing the D_2 to react to form DBr, and (2) interaction of D_2 with the graphite electrode to produce hydrocarbons (*e.g.*, CD_4 or C_2D_2).

When a ceramic-coated graphite electrode is used, D_2 is generated only above 2.5 V, but the D_2 recovery efficiency is greatly improved. For the particular experiment shown in Fig. 19, 93% of the deuterium was recovered as D_2. This high recovery efficiency is typical of extraction experiments carried out down to 1 wppm deuterium. In comparing the experimental results for the two electrodes, an obvious feature is the different rates at which D_2 is generated. The coated electrode generated D_2 much faster than the uncoated electrode, possibly because the ceramic layer inhibits back reaction of the D_2 with Li in the salt. However, the ceramic most likely stabilizes a polarization layer around the electrode which accounts for the much higher potential required to liberate the D_2 as compared with the potential required with the uncoated electrode.

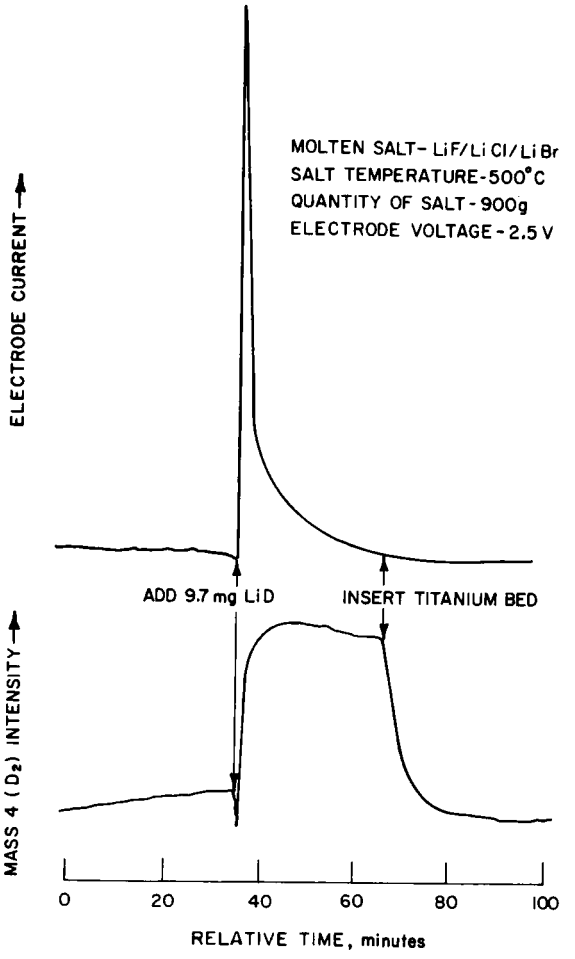

Fig. 19. Results of a Typical Electrochemical Experiment to Evolve Deuterium, Using a Ceramic-Coated Graphite Electrode

It is apparent from the electrochemical experiments completed to date that back reaction of D_2 with the lithium which saturates the molten salt can be successfully prevented using a sparged electrode. Recovery of hydrogen isotopes down to 1 wppm is easily achieved, as has been demonstrated. Problems that have been encountered are most likely attributable to the use of graphite as the electrode material. It is reasonable to anticipate even better performance with the sintered stainless steel electrode now under study. If this is realized, electrochemical evolution will, in all probability, be the preferred method for recovery of hydrogen isotopes from molten-salt extractants.

C. Lithium-Processing Test Loop

(J. R. Weston, S. B. Skladzien, R. Malecha, and V. A. Maroni)

With the successful demonstration of bench-scale experiments for (1) the molten-salt extraction of tritium from lithium and (2) the recovery of hydrogen isotopes from selected molten salts, plans are being made to build

a facility that integrates these experiments into an extraction processing system. A multipurpose lithium-processing test loop (LPTL) has been designed. The 50-gallon forced-circulation loop will be used to (1) test the effectiveness of semi-continuous molten-salt extraction, using a single vessel as a pseudo mixer-settler; (2) evaluate the efficiency of an elevated-temperature getter trap (probably containing zirconium) and a thermally regenerative cold trap (in series with the getter trap) for removing nonmetallic element impurities from lithium; and (3) develop impurity control, process, and monitoring methodology for large liquid lithium loop systems. Provisions have been made in the design for the attachment of additional experimental test sections, *e.g.*, monitoring devices, other types of gettering materials, and heat-exchanger mock-ups. A simplified schematic drawing of the processing loop is shown in Fig. 20. The facility is being fabricated from 304L stainless steel and will operate at or below 550°C. Construction of the loop components is under way, and operation is expected to begin in the fall of 1977.

D. Lithium Mini-Test Loop

(R. M. Yonco and J. R. Weston)

A lithium mini-test loop having a capacity of about one liter of lithium has been constructed to support the design of the 50-gallon lithium-processing test loop (LPTL). This loop will be used to test the performance of the Nupro 8U series valves chosen for LPTL, establish operating parameters for the heated zirconium getter traps, and establish lithium-sampling procedures.

A diagram of the loop is shown in Fig. 21. The reservoir is made of 304 SS, and all other components in contact with molten lithium are made of 316 SS. All joints in the main loop are welded and vacuum tight. The flow of lithium is from the bottom of the reservoir to the electromagnetic pump and the dc flowmeter, through either of the two Nupro valves, to the heated zirconium getter trap, and back to the reservoir. A helium atmosphere is maintained in the head space above the molten lithium.

The heated zirconium getter trap is located in a side arm of the loop and is intended to reduce the oxygen and nitrogen content of the lithium. The trap will be operated at temperatures up to about 650°C; the active material consists of twenty-four 15-in. lengths of 1/16-in. zirconium wire.

The entire loop and reservoir are wrapped in a close-fitting stainless steel screen which is electrically insulated from the loop by a layer of asbestos. In the event of a lithium leak, electrical contact will be made between the loop and the screen by the escaping lithium and all power to the loop will be shut off by interlocking circuitry in the control console.

The loop is heated by the getter furnace and by three circuits of heating wire wrapped around the reservoir, the getter side arm, and the connecting tubing. The temperature can be monitored at seven locations by thermocouples fastened to the loop. Temperature gradients are established by adjusting the heat input at any of the four sources, by varying the insulation around the loop, and by adjusting the flow rate of lithium through the loop.

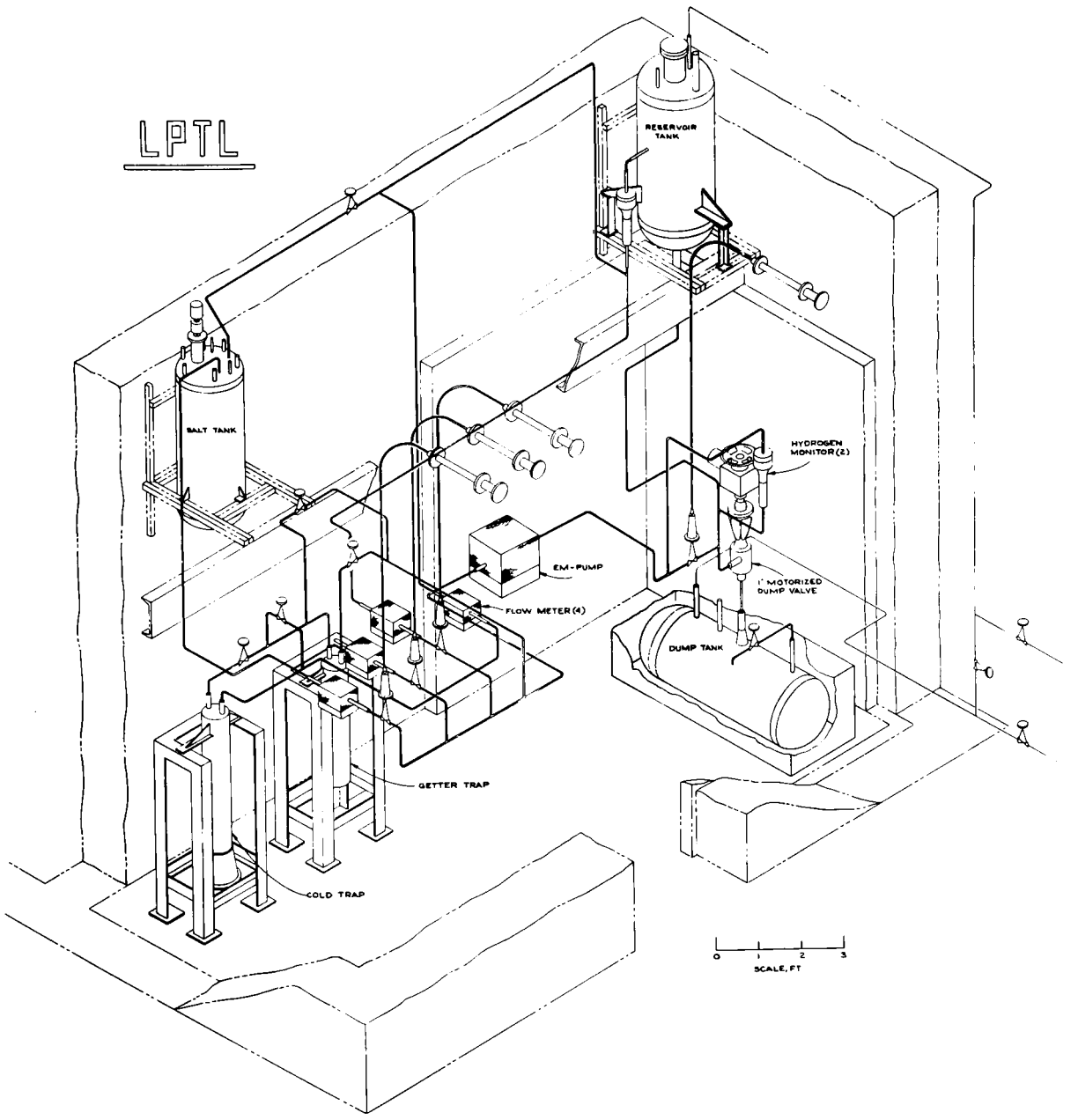

Fig. 20. Simplified Schematic of Lithium-Processing Test Loop

Lithium is added to the loop by filling the transfer tank with clean lithium in a helium glove box, connecting the cooled tank to the fill tube and manifold, equalizing the head pressure in the tank and the reservoir, and melting the lithium in the tank, thereby causing the lithium to flow into the reservoir. The goose neck of the fill tube then forms a freeze plug to seal off the reservoir.

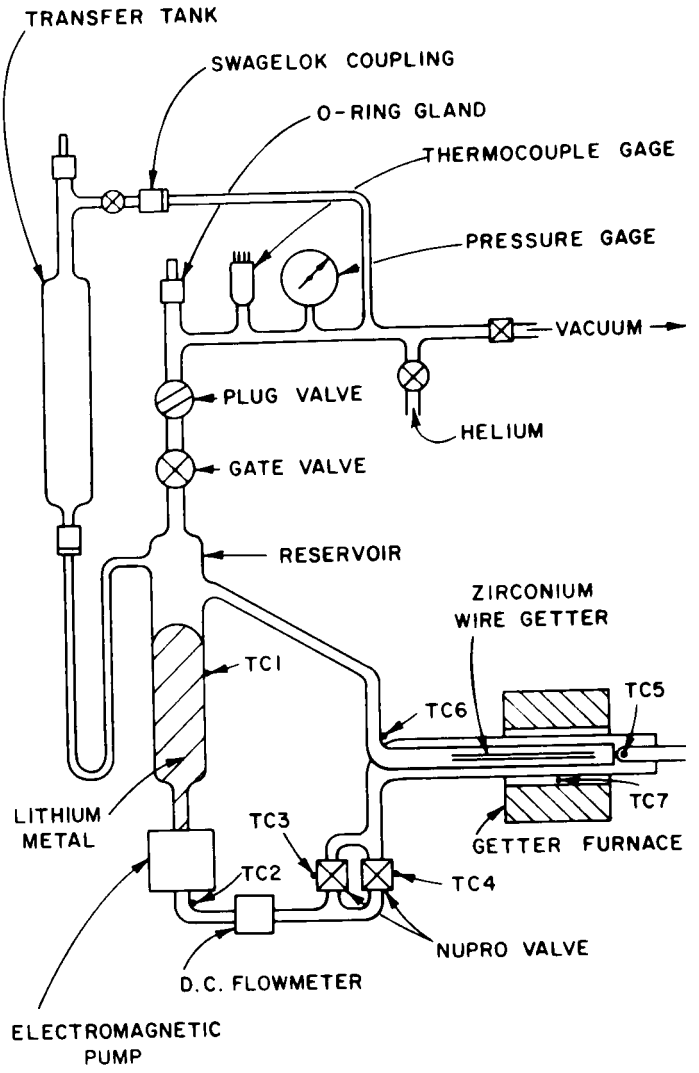

Fig. 21. Lithium Mini-Test Loop

Sampling of the liquid lithium in the reservoir is accomplished by placing a sampling tube attached to a rod in the transfer lock formed by the O-ring seal around the rod, the plug valve, and the manifold. The lock is flushed with helium, and the sampling tube lowered into the reservoir. By cycling the pressure, the immersed tube is filled with lithium and withdrawn from the reservoir through the lock.

The overall space requirements for the loops are height, 3 ft; depth, 2 ft; and width, 4 ft; which allows the loop to be located in a Kewanee hood. Supporting facilities and controls are located outside the hood, and include four controlled power supplies, a multipoint temperature recorder, vacuum gauge, flow meter, and safety circuitry that will cut off all power to the loop in the event of loss of lithium flow, lithium leakage, loop temperature excursion, or smoke detection.

REFERENCES

1. Chemical Engineering Division Liquid Metals Chemistry and Tritium Control Technology Annual Report, July 1974-June 1975, Argonne National Laboratory Report ANL-75-50 (1975).

2. Chemical Engineering Division Physical Inorganic Chemistry Annual Report, July 1973-June 1974, Argonne National Laboratory Report ANL-8123 (1974).

3. Chemical Engineering Division Physical Inorganic Chemistry Semiannual Report, January-June 1973, Argonne National Laboratory Report ANL-8023 (1973).

4. Chemical Engineering Division Physical Inorganic Chemistry Semiannual Report, July-December 1972, Argonne National Laboratory Report ANL-7978 (1972).

5. V. A. Maroni *et al.*, Experimental Studies of Tritium Barrier Concepts for Fusion Reactors, Proceedings of the International Conference on Radiation Effects and Tritium Technology for Fusion Reactors, Gatlinburg, TN, Oct. 1-3, 1975, CONF-750989, U. S. Energy Research and Development Administration, Vol. IV, p. 329 (1976).

6. W. F. Calaway *et al.*, A Review of the ANL Program on Liquid Lithium Processing and Tritium Control Technology, Proceedings of the Second ANS Topical Meeting on the Technology of Controlled Nuclear Fusion, Richland, WA, September 21-23, 1976.

7. V. A. Maroni, J. Nucl. Mater, 53, 293 (1974).

8. R. R. Heinrich, C. E. Johnson, and C. E. Crouthamel, J. Electrochem. Soc, 112, 1071 (1965).

9. R. L. Schulte, High Resolution Depth Profiling of Oxygen and Carbon in Materials by Spectral Deconvolution, Nucl. Instrum. Methods (in press).

10. R. L. Schulte and M. C. Stauber, Grumman Aerospace Corporation, Bethpage, New York (personal communication).

11. E. H. Van Deventer *et al.*, Effects of Surface Impurity Layers on the Hydrogen Permeability of Vanadium, J. Nucl. Mater, 64, 241 (1977).

12. R. W. Webb, Permeation of Hydrogen through Metals, USAEC Report, NAA-SR-10462, (July 1965).

13. Nuclear Systems Material Handbook, USERDA Report TID-2666, Vol, I, Part 1, Section 2, Code 3112.

14. W. H. McAdams, Heat Transmission, McGraw-Hill Book Co. (1954).

15. W. M. Stacey, Jr., *et al.*, Tokamak Experimental Power Reactor Conceptual Design, Argonne National Laboratory Report ANL/CTR-76-3 (August 1976).

16. W. M. Stacey, Jr., Tokamak Engineering Technology Facility Scoping Study, Argonne National Laboratory Report ANL/CTR-76-1, (March 1976).

REFERENCES

17. R. H. Perry and C. H. Chilton, Chemical Engineers Handbook, McGraw-Hill Book Co., New York (1973).

18. N. R. Amundson, Mathematical Methods in Chemical Engineering, Matrices and Their Applications, Prentice Hall, New York (1966).

19. B. D. Smith, Design of Equilibrium Stage Processes, McGraw-Hill Book Co., New York (1963).

20. H. M. Mittelhauser and G. Thodos, Vapor Pressure Relationship up to Critical Point of Hydrogen Deuterium and Tritium, and Their Atomic Combinations, Cryogenics, 4, 368 (1964).

21. B. Misra and V. A. Maroni, Multicomponent Isotopic Separation and Recirculation Analysis, Argonne National Laboratory Report ANL-76-92 (1977).

22. V. A. Maroni, R. D. Wolson and G. E. Staahl, Nucl. Technol. 25, 83-71 (1975).

23. E. Veleckis and V. A. Maroni, Thermodynamic Properties of Solutions of Hydrogen Isotopes in Metals and Alloys of Interest to Fusion Reactor Technology, Proceedings of the International Conference on Radiation Effects and Tritium Technology for Fusion Reactors, Gatlinburg, TN CONF-750989, U. S. Energy Research and Development Administration, Vol. III, p. 458 (1976). Oct. 1-3, 1975.

24. V. A. Maroni, E. J. Cairns and F. A. Cafasso, A Review of the Chemical, Physical and Thermal Properties of Lithium that are Related to its Use in Fusion Reactors, Argonne National Laboratory Report ANL-8001 (1973).

25. P. A. Nelson *et al.*, Development of High Specific Energy Batteries for Electric Vehicles, Progress Report, August 1973-January 1974, Argonne National Laboratory Report ANL-8058 (1974).

26. R. N. Seefurth and R. A. Sharma, J. Electrochem. Soc. 122, 1049-1053 (1975).

27. D. A. J. Swinkels, Electrochem. Technol. 5, 396-397 (1967).

Distribution of ANL-76-133

Internal:

M. V. Nevitt
D. L. Smith
W. M. Stacey
E. G. Pewitt
L. Burris (4)
F. A. Cafasso
W. F. Caloway
R. G. Clemmer
L. Cuba
A. K. Fischer
G. M. Kesser
V. A. Maroni (30)
J. M. McKee
C. C. McPheeters
A. Melton
B. Misra
D. J. Raue
T. A. Renner
J. Royal
S. B. Skladzien
R. K. Steunenberg
E. Van Deventer
E. Veleckis
R. M. Yonco
A. B. Krisciunas
ANL Contract Copy
ANL Libraries (5)
TIS Files (6)

External:

ERDA-TIC, for distribution per UC-20 (190)
Manager, Chicago Operations Office
Chief, Chicago Patent Group
President, Argonne Universities Association
Chemical Engineering Division Review Committee:
R. C. Axtmann, Princeton U.
R. E. Balzhiser, Electric Power Research Inst.
J. T. Banchero, U. Notre Dame
D. L. Douglas, Gould Inc.
P. W. Gilles, U. Kansas
R. I. Newman, Allied-General Nuclear Services
G. M. Rosenblatt, Pennsylvania State U.